

MICROWAVE CHARACTERIZATION OF LOW-K
DIELECTRIC THIN FILMS USING MICROSTRIP
TRANSMISSION LINES

THESIS

Presented to the Graduate Council of
Southwest Texas State University
in Partial Fulfillment of
the Requirements

For the Degree
Master of SCIENCE

By
Kevin Patrick Radican, B.S.

San Marcos, Texas
May, 2003

ACKNOWLEDGMENTS

First I would like to thank my parents David and Esther Radican for their selflessness in both financing my academic career, and in their endless support.

I would also like to thank Dr. Heather C. Galloway and Dr. James Crawford. Without their help I would have been expelled from school a long time ago.

In addition I'd like to thank the faculty of the SWT physics department, especially Dr. David W Donnelly, Dr. Heather C. Galloway, Dr. Wilhelmus J. Geerts, Ms. Pat Parks, and Dr. Greg Spencer, for sharing their knowledge and wisdom, without which this project would not have been successful.

To finish I would like to thank the members of my thesis committee, Gary W. Beall, Dr. David W Donnelly, and Dr. Heather C. Galloway, for their time and help with this thesis.

TABLE OF CONTENTS

LIST OF TABLES	vii
LIST OF FIGURES.....	viii
ABSTRACT	x
Chapter	
1 INTRODUCTION.....	1
2 MEASURING THE DIELECTRIC PROPERTIES OF LOW-K THIN FILMS	4
2.1 A General Theory of Microstrips.....	4
2.2 The Calibration Comparison Method.....	7
2.3 Characterization of a Microstrip Transmission Line.....	15
2.4 TRL Calibration Standard Design Considerations.....	17
3 FABRICATION PROCESS.....	20
3.1 Basic Outline for the Fabrication Process.....	21
3.2 DC Magnetron Sputter Deposition	23
3.3 Photolithography.....	25
3.4 Wet Etch	30
3.5 Strip.....	31
3.6 Plasma Etch	31
4 PLASMA ETCH RATE STUDY.....	33
4.1 Reactive Ion Etching	34
4.2 Experimental Setup.....	37
4.3 Etch Rate Results	40
4.4 Etch Study Conclusion.....	47
5 MICROWAVE ELECTRICAL MEASUREMENTS	48
5.1 Cascade Microwave Probe Station.....	48

5.2 Agilent 8719ES Network Analyzer	50
5.3 NIST MultiCal.....	51
6: CONCLUSIONS.....	53
6.1 Etch Study.....	53
6.2 Microstrip Transmission Lines	54
APPENDIX A: OUTLINE OF FAB PROCESS	56
APPENDIX B: OPERATING PROCEDURES.....	58
APPENDIX C: LASER WRITER CODE.....	66
APPENDIX D: MICROSTRIP ϵ_{eff} CALCULATION.....	118
GLOSSARY	120
BIBLIOGRAPHY.....	122
VITA	124

LIST OF TABLES

Number

1. Definitions of s-parameters..... 6
2. SiC etch depth in angstroms over time at different oxygen concentrations..... 41
3. Average SiC Etch Rate at various oxygen concentrations..... 42
4. Etch rates of various fluorinated gasses 42
5. Si and Al Etch Rates at various oxygen concentrations..... 43
6. DC resistance and capacitance of microstrip lines 55

LIST OF FIGURES

<i>Number</i>	<i>Page</i>
1. Top view of a microstrip transmission line.....	2
2. Cross section of a low-k wafer.....	3
3. Cross section of a microstrip on a low-k wafer	3
4. Block Diagram of S-parameters for a device	7
5. Schematic of a device under test (DUT)	7
6. Schematic of a test network	8
7. The equivalent circuit model for the contact pads	16
8. Transmission line equivalent circuit model.....	16
9. AppCad window used to calculate a thru standard on SiC	19
10. AppCad window for a 4250 micron line standard on SiC.....	19
11. Ground lines etched in aluminum.....	21
12. Side view of the sample after plasma etching	22
13. Top View of SiC after plasma	22
14. Aluminum Microstrip lines	23
15. Cross section of microstrip	23
16. Schematic of magnetron gun	24
17. View of magnetron chamber	24
18. Laurell Technologies Corp. WS-400A-6NPP-LITE spinner.....	26

19. Inside view of laser writer	28
20. Schematic of laser writer	29
21. HFC 134a molecule	33
22. Samples being etched in the magnetron gun by a plasma	38
23. Two samples in the magnetron gun before etching.....	38
24. Photo of features.....	38
25. Schematic of an impedance matching	39
26. SiC etch rates over time at different oxygen flow.....	44
27. Graph of etch rate vs. oxygen flow.....	44
28. Graph of bias voltage vs. oxygen flow	45
29. AFM image of trench etched in SiC	45
30. AFM image of the bottom of an etched SiC feature.....	46
31. AFM image of cross-section of the etched trench in SiC.....	46
32. Cascade Microtech microwave probe station	49
33. Picture of the open air coplanar probe contacting thru standard.....	49
34. Agilent 8719ES VNA	50
35. AFM image of aluminum microstrip line on SiC.....	55

ABSTRACT

MICROWAVE CHARACTERIZATION OF LOW-K DIELECTRIC THIN FILMS USING MICROSTRIP TRANSMISSION LINES

by

Kevin Patrick Radican, B.S., Physics

Southwest Texas State University

May 2003

Supervising Professor: Heather C. Galloway

In order to reduce the effects of the parasitic RC time delay the microelectronics industry is moving to low-k dielectric materials for use with metal lines in future integrated circuit chips, as outlined by the International Technology Roadmap for Semiconductors. The high frequency electrical properties of these new low-k materials are not always well known. This thesis presents a method to study the electrical properties of several candidate low-k materials at frequencies of 0.5 to 13.5 GHz using microstrip transmission lines both before and after chemical mechanical planarization (CMP). The microstrips are fabricated on wafer samples consisting of a 300 nm low-k thin film, and 100 nm SiC interlayer, using DC magnetron sputtering, laser beam photolithography, and reactive ion etching. In order to etch through the SiC under layer for a proper ground contact with the substrate, a reactive ion plasma etch

process using RF magnetron sputtering with tetrafluoroethane and oxygen gases was also developed. A SiC etch rate with respect to oxygen concentration investigation was also entailed in this thesis. The electrical properties were measured with an Agilent 8719ES network analyzer and a Cascade Microtech microwave probe station.

Chapter 1

INTRODUCTION

As clock frequency in modern IC's steadily increases according to Moore's law the parasitic RC time delay inherent in metal lines is becoming an obstacle. These problems can be minimized through decreasing resistance, R , or capacitance, C . Resistance can be decreased by using metal lines with lower resistance such as Cu in making interconnects. Capacitance ($C \sim \epsilon/d$) can be lowered two ways. By lowering the dielectric constant k of the insulator, or increasing the distance d between the capacitor's plates. The distance d is decreasing as chips are scaled down so k must be lowered in order to decrease C . The most common insulator used today is SiO_2 with a k of 3.9. Low- k dielectrics are materials with a k less than 3.5. These new materials need to be characterized at microwave frequencies to determine applicability in tomorrow's faster IC's. We are investigating the high frequency characteristics of two porous methyl silsesquioxane (MSQ) based organosilicate glass (OSG) spin on low- k dielectrics, whose trade names are CORAL and SiLK. These materials will be evaluated before and after chemical mechanical planarization, CMP, using a microstrip transmission line.

A microstrip transmission line is an electrical circuit designed to efficiently transmit electromagnetic (EM) energy at high frequencies where traditional circuits become inefficient.

A microstrip is designed to propagate EM excitations in a wave mode with the electric and the magnetic field vectors transverse to the direction of energy transfer, or TEM mode. A microstrip transmission line or simply a microstrip consists of a metal signal line with two ground return lines on either side. This is described as a ground signal ground configuration or GSG. The microstrip is fabricated on top of the samples of interest. The electrical characteristics of this microstrip are dependent on the electrical properties of the underlying materials; measurements can then be made to characterize the microstrip giving information about the materials of interest.

In the move to Cu/low-k, the metal lines of the wafers will have a SiC under layer between the Si substrate and the low-k. This layer acts as a diffusion barrier for the Cu. In order to reduce the resistance of the ground return through the substrate, coplanar waveguide like metal rails were built between the ground pads with an ohmic contact to the substrate. To do this a small trench or via had to be etched through the low-k and the SiC. Silicon carbide is a rather chemically resistant material and is typically etched with a fluorinated plasma. As a result of this a method of etching SiC had to be developed and is also discussed in this work.

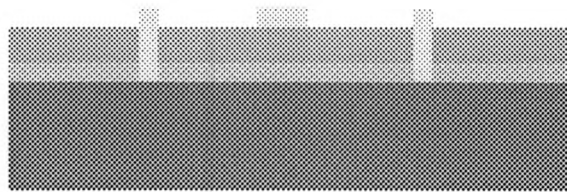


Figure 1 Cross section of a microstrip on a low-k wafer showing the ground lines contacting the Si substrate

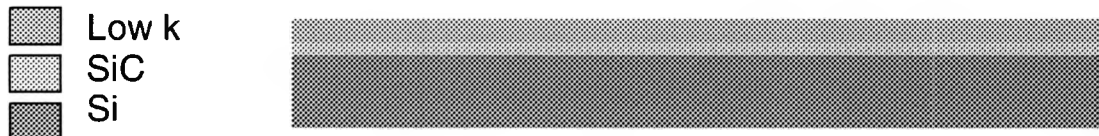


Figure 2. Cross section of a low-k wafer before device construction

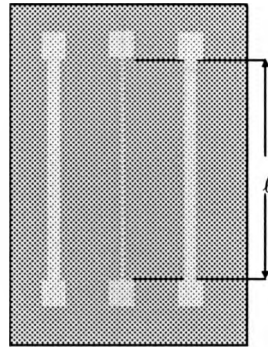


Figure 3. Top view of a microstrip transmission line. The outer two lines are the ground planes, and the middle is the signal line. The contact pads are the squares located at the ends of each line.

Chapter 2

MEASURING THE DIELECTRIC PROPERTIES OF LOW-K THIN FILMS

2.1

A General Theory of Microstrips

A microstrip directs electromagnetic excitations to provide efficient energy transfer, and to permit only one mode of propagation, called a transverse electric and magnetic (TEM) mode. In the TEM mode the electric and magnetic field vectors are both normal to the direction of propagation. The EM field pattern of a mode depends on the excitation frequency, dielectric constants, and microstrip geometry. These modes satisfy Maxwell's equations in a source-free region and the analytic procedure for finding the microstrip fields and propagation constants is to solve these wave equations for the z-components of the fields, subject to the boundary conditions for the microstrip, and then find the transverse field components. It is important to note that there are some important differences between microstrip circuits and classic electrical circuits. For instance, the high frequency microstrip current and voltage, unlike its classical electrical counter part are dependent on definition and

normalization. Also, unlike low frequency electrical circuits, microstrips must be described in terms of traveling waves [1]. The classical definition of the microstrip current and voltage is only applicable to modes that are transverse electric (TE), transverse magnetic (TM), and TEM. In our case of a microstrip with nonuniform material parameters, i.e. multiple dielectric layers and a lossy dielectric substrate the modes are generally hybrid rather than TE, TM, or TEM. This classical theory fails for this case, and a more practical method of microstrip characterization is to take an engineering approach. Assuming that in a hybrid TEM mode the conventional microstrip voltage and current follow the same telegrapher's equation (equation 1) that governs propagation in a low frequency transmission line (equation 1) where V is voltage, I is current, j is the square root of -1, ω is the angular frequency.

$$\begin{aligned} -dV(z)/dz &= (R + j\omega L) I(z) \\ -dI(z)/dz &= (G + j\omega C) V(z) \end{aligned} \quad \text{Equation 1}$$

The characteristic impedance can be written in terms of equivalent circuit parameters capacitance C , conductance G , inductance L , and resistance R , by $j\omega C + G = \frac{\gamma}{Z_0}$ and $j\omega L + R = \gamma Z_0$ [21]. However, this method overlooks an important difference between high frequency microstrips and low frequency transmission lines. High frequency microstrip voltages and currents are inaccessible experimentally and high frequency instrumentation is based on measurements of waves and their complex power, $p = v i^*$, where v is the voltage and i is the current. The scattering matrix S relates these traveling wave intensities, called scattering parameters, instead of the circuit voltages and currents as in the classic impedance matrix. Scattering parameters called S-parameters are a convention used to characterize the way a device modifies signal flow. The S-parameters for a two-port network are defined using the

reflected or emanating waves, b_1 and b_2 , as the dependent variables, and the incident waves, a_1 and a_2 , as the independent variables. The general equations for these waves as a function of the S-parameters are shown below:

$$\begin{aligned} b_1 &= S_{11}a_1 + S_{12}a_2 \\ b_2 &= S_{21}a_1 + S_{22}a_2 \end{aligned} \quad \text{Equation 2}$$

S-Parameter	Definition	Test Set Description	Direction
S_{11}	$b_1/a_1, a_2 = 0$	Input reflection coefficient	FWD
S_{21}	$b_2/a_1, a_2 = 0$	Forward gain	FWD
S_{12}	$b_1/a_2, a_1 = 0$	Reverse Gain	REV
S_{22}	$b_2/a_2, a_1 = 0$	Output reflection coefficient	REV

Table 1 Definitions of s-parameters

Using these equations, the individual S-parameters can be determined by taking the ratio of the reflected or transmitted wave to the incident wave with a perfect termination placed at the output. For example, to determine the reflection parameter from Port 1, defined as S_{11} , we take the ratio of the reflected wave b_1 to the incident wave a_1 using a perfect termination on Port 2. The perfect termination guarantees that $a_2 = 0$ since there is no reflection from an ideal load. The remaining S-parameters, S_{21} , S_{22} and S_{12} , are defined in a similar manner [2]. These four S-parameters completely define the two-port network characteristics. The network analyzer used in measurement measures a “pseudo-wave” defined with respect to a reference impedance Z_r that is not necessarily related to the characteristic impedance Z_0 . The measured pseudo wave need not be the actual traveling wave and therefore cannot be interpreted as such [1]. The pseudo-waves reduce to the traveling waves when $Z_r = Z_0$.

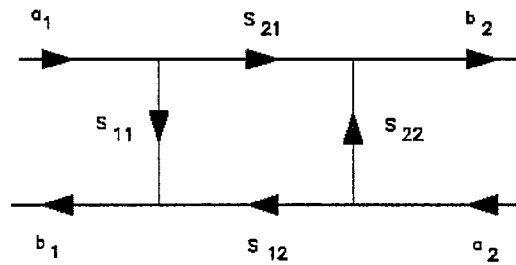


Figure 4 Block Diagram of S-parameters for a device

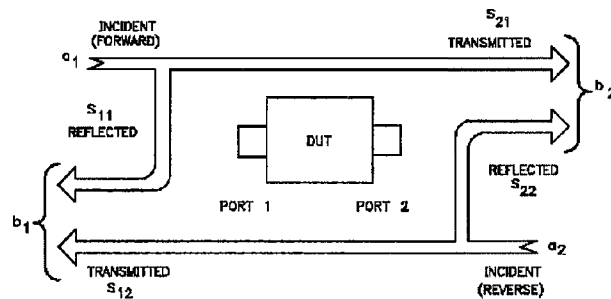


Figure 5 Schematic of a device under test (DUT) The subscripts denote the port number. The letter a defines a forward wave and b defines a reflected wave.

2.2

The Calibration Comparison Method

The calibration comparison method is a de-embedding algorithm that is used to calibrate out the electrical effects of the measurement fixture, and to extract the characteristic impedance from the device under test, or DUT. The test equipment used for characterizing the microwave properties of the microstrip lines is a vector network analyzer (VNA), which uses standard 50 Ω coaxial interfaces at the test ports. The test equipment is calibrated at the

coaxial interface defined as the “measurement plane,” and the required measurements are at the point where the probe tips contact to the microstrip pads, or the “device plane”. When the VNA is calibrated at the coaxial interface using any standard calibration kit, the DUT measurements include the test fixture effects. De-embedding uses a model of the test fixture and mathematically removes the fixture characteristics from the overall measurement.

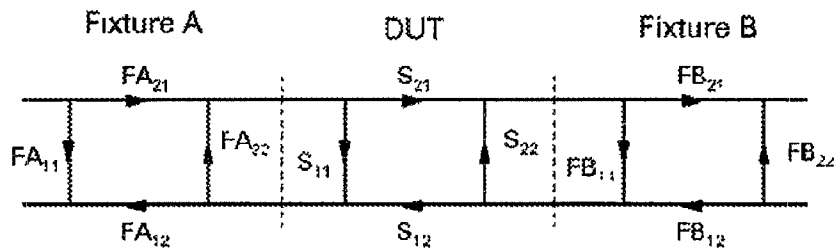


Figure 6 Schematic of a test network divided in to three separate s-matrices. Two of the matrices, Fixture A and Fixture B, define the left and right of the test fixture, and the DUT matrices defines the device.

The fixture and device can be represented as three separate two-port networks. In this way, the test fixture is divided in half to represent the coaxial to non-coaxial interfaces on each side of the DUT. The two fixture halves will be designated as Fixture A and Fixture B for the left-hand and right-hand sides. The S-parameters FA_{xx} and FB_{xx} ($xx = 11, 21, 12, 22$) will be used to represent the S-parameters for the left half and right half of the test fixture, and S_{xx} will be used to represent the microstrip.

To directly multiply the matrices of the three networks, it is mathematically advantageous to convert the S-parameter matrices to scattering transfer matrices or T-parameters. The mathematical relationship between S-parameter and T-parameter matrices is given by equation 3.

$$\begin{bmatrix} S_{11} & S_{12} \\ S_{21} & S_{22} \end{bmatrix} = \begin{bmatrix} \frac{T_{12}}{T_{22}} & \frac{T_{11}T_{22} - T_{12}T_{21}}{T_{22}} \\ \frac{1}{T_{22}} & -\frac{T_{21}}{T_{22}} \end{bmatrix} \quad \text{Equation 3}$$

The two-port T-parameter matrix can be represented as [T], where [T] is defined as having the four parameters of the network.

$$[T] = \begin{bmatrix} T_{11} & T_{12} \\ T_{21} & T_{22} \end{bmatrix} \quad \text{Equation 4}$$

Because the test fixture and DUT are defined as three cascaded networks, their respective T-parameter networks, T_A, T_{DUT} and T_B can be easily multiplied. This matrix operation will represent the T-parameters of the test fixture and DUT when measured by the VNA at the measurement plane.

$$[T_{\text{MEASURED}}] = [T_A] [T_{\text{DUT}}] [T_B] \quad \text{Equation 5}$$

Using matrix theory if a matrix determinant is not equal to zero, then the matrix has an inverse, and any matrix multiplied by its inverse will result in the identity matrix. So if we multiply the following T-parameter matrix by its inverse matrix, we obtain the identity matrix. given in equation 6.

$$\begin{bmatrix} \mathbf{T} \end{bmatrix} \begin{bmatrix} \mathbf{T} \end{bmatrix}^{-1} = \begin{bmatrix} 1 & 0 \\ 0 & 1 \end{bmatrix} \quad \text{Equation 6}$$

To de-embed the two sides of the fixture, T_A and T_B , and gather the information from the DUT or T_{DUT} we can apply this matrix inversion. We can multiply each side of the measured result by the inverse T-parameter matrix of the fixture and yield the T-parameter for the DUT only. The T-parameter matrix can then be converted back to the desired S-parameter matrix. Using the S or T-parameter model of the test fixture and VNA measurements of the total combination of the fixture and DUT, we can apply the matrix equation 6 to de-embed the fixture from the measurement. The de-embedding process is typically implemented after the measurements are captured from the VNA

$$\begin{bmatrix} T_A \end{bmatrix}^{-1} \begin{bmatrix} T_A \end{bmatrix} \begin{bmatrix} T_{DUT} \end{bmatrix} \begin{bmatrix} T_B \end{bmatrix} \begin{bmatrix} T_B \end{bmatrix}^{-1} = \begin{bmatrix} T_{DUT} \end{bmatrix} \quad \text{Equation 7}$$

The most accurate method of VNA calibration is TRL [3,4], a moniker that refers to the use of a “thru,” and “reflect,” and a “line.” The thru is a length of transmission line which connects at either end to a test port. The line standard is a longer section of transmission line. The reflect is a symmetric and transmissionless but otherwise arbitrary two-port device embedded in a section of transmission line. The method assumes that each measured device has an identical transition from the test port to the calibration reference plane. The reference planes are set to the center of the thru.

The calibration comparison method for on-wafer calibrations [5] is a de-embedding algorithm based on the two-tier TRL calibration [6] and determines the two fixture T-matrices, or "error boxes" by relating two on-wafer calibrations. Typically, these matrices represent the relationship between a first- and a second-tier calibration. Once these matrices have been determined, several important quantities can be derived that quantify the systematic differences between the two calibrations. Most important are changes in the reference plane position and reference impedance, but another important application of the calibration comparison method is the determination of the characteristic impedance Z_0 of planar transmission lines printed on lossy substrates [7]. Z_0 can be found even when contact-pad capacitance and conductance are large. The method begins with the performance of a multiline TRL probe-tip calibration [1] using a set of easily characterized reference lines. The reference impedance of this calibration set is 50Ω , and its reference plane is moved back to the device plane. A second-tier multiline TRL calibration in the transmission lines of interest determines the error boxes relating it to the 50Ω probe-tip calibration.

A two-port VNA in which the switching and isolation errors are either negligible or have been completely accounted for by some correction algorithm provides a measurement M_i of the product of three matrices [1]

$$M_i = XT_i\bar{Y} = T_A T_{DUT} T_B \quad \text{Equation 8}$$

where the reverse cascade matrix of Y is

$$\bar{Y} = \begin{bmatrix} 01 \\ 10 \end{bmatrix} Y^{-1} \begin{bmatrix} 01 \\ 10 \end{bmatrix}, \quad \text{Equation 9}$$

and T_i is the cascade matrix of device i . The calibration procedure consists of connecting a number of devices whose cascade matrices T_i are assumed to be known. When enough measurements M_i are available, approximations to the matrices X and Y are determined.

Let T^M be the cascade matrix of a device measured with respect to a calibration M , T^B its cascade matrix measured with respect to a benchmark calibration, and T^0 its actual cascade matrix. Then equation 14 shows that T^M , T^B , and T^0 must be related by

$$T^M = X^B T^B \bar{Y}^B = X^0 T^0 \bar{Y}^0. \quad \text{Equation 10}$$

The matrices X^0 , T^0 , X^B , and Y^B are independent of the device under test and are determined by the calibrations. The verification is based on determining these matrices.

The verification begins with a VNA calibrated with initial calibration M . Subsequently, a benchmark calibration based on precise transmission lines is performed with respect to calibration M using the two-tier multi-line TRL calibration of Marks [8]. This procedure determines X^B and Y^B . Marks and Williams [1] show that the TRL calibration provides a direct measurement of the cascade matrix T^0 when the same lines and transitions connected to the device under test are used in the calibration and when there are no random measurement errors or unaccounted-for switching and isolation errors. They also show that those cascade parameters are measured with respect to a reference plane in the center of the thru line, whose length we designate $2l_0$, and a reference impedance which is equal to the characteristic impedance Z_0 of the line. Since this is true for all devices embedded in the line, $T^B = T^0$ for all matrices T^0 , and therefore $X^B = X^0$ and $Y^B = Y^0$. This is true only when the same transitions and

lines connected to the device are employed in the TRL calibration procedure. Thus the “correct” benchmark is the TRL calibration using the same lines and transitions as are actually connected to the device.

The matrices X^0 and T^0 describe the differences between measurements performed with respect to the initial calibration M and the actual S-parameters of the device. If the calibration M measures the actual S-parameters, then $X^0=Y^0=I$, the identity matrix. Deviations from the identity matrix may occur for a number of reasons. For instance, a TRL calibration may not be perfect due to random connector and other measurement error. In that case, X^0 and Y^0 represent these random errors.

The TRL method, like other calibration methods, determines the matrices X^m and Y^n . However, these two matrices are nonunique since they depend on the reference impedances. Thus, we need to analyze the algorithm to determine which reference impedances are imposed by the calibration. Our first standard ($i=1$), an ideal thru, is a continuous connection between two identical lines. Since the traveling waves are not disturbed, the cascade matrix using a reference impedance of Z_0 must be the identity matrix I :

$$T_1^0 = I \quad \text{Equation 11}$$

The algorithm imposes the condition that the reference impedances on both ports be identical. The thru alone cannot provide any information as to the value of the reference impedance.

Another result of the TRL algorithm is that the calibrated measurement of the reflect standard is identical on both ports. This again reveals nothing about the port reference

impedances except that they are identical. The ideal line standard ($i = 2$) is a length of transmission line identical to that of the two test ports and connected to them without discontinuity. As a result, there is no reflection of the traveling waves. This requires the cascade matrix of the line, with a reference impedance of Z_0 , to be

$$T_2^0 = \begin{bmatrix} e^{-\gamma l} & 0 \\ 0 & e^{+\gamma l} \end{bmatrix} \quad \text{Equation 12}$$

where γ is the propagation constant and l is the line length. The TRL algorithm ensures that the cascade matrix is diagonal and therefore that the calibrated measurement of the line will be such that $S_{11} = S_{22} = 0$. That is, the TRL method using a perfect line and thru results in a consistent calibration with identical reference impedances on each port equal to the characteristic impedance of the line. Recall that the condition $Z_{ref}^m = Z_0$ was the condition under which the pseudo-waves are equal to the actual traveling waves. Thus the TRL method calibrates the VNA so as to measure the unique scattering matrix S^0 which relates the actual traveling waves, not some arbitrary pseudo-scattering matrix S .

2.3

Characterization of a Microstrip Transmission Line

Before we can mathematically de-embed the test fixture from the device measurements, the S or T-parameter network for each fixture half needs to be modeled. Reference [7] suggests a different treatment of the error boxes determined by [5], which is insensitive to contact pad parasitics and is well suited for determining the characteristic impedance on lossy substrates. The model used when contact pad capacitances are large is called the contact pad model. This algorithm is used to determine Z_o of transmission lines on lossy silicon substrates with the calibration comparison method [2]. The method increases measurement accuracy by automatically accounting for shunt contact-pad capacitance and conductance, reducing them as sources of systematic error [8]. Figure 7 shows a simple model for a probe tip to transmission line transition [8]. The model consists of a lossy shunt contact-pad with admittance Y in parallel with an impedance transformer mapping the reference impedance Z_r of the probe tip calibration into the reference impedance Z_o of the second-tier TRL calibration. The transmission matrix X of the circuit in Figure 7 is

$$X = \frac{1}{\sqrt{1-\Gamma^2}} \left(\begin{bmatrix} 1 & \Gamma \\ \Gamma & 1 \end{bmatrix} + (1+\Gamma) \frac{YZ_r}{2} \begin{bmatrix} -1 & -1 \\ 1 & 1 \end{bmatrix} \right) \quad \text{Equation 13}$$

where $\Gamma \equiv \frac{Z_0 - Z_r}{Z_0 + Z_r}$. The calibration comparison method estimates $\Gamma_0 = \sqrt{\frac{X'_{12} X'_{21}}{1 + X'_{12} X'_{21}}}$ and it shows that while Γ_0 may not be sensitive to these reference plane transformations, Y is [8].

This is corrected by the new method by using the estimate $\Gamma_1 \equiv \sqrt{\frac{(X'_{12} + X'_{21})^2}{4 + (X'_{12} + X'_{21})^2}}$ which is insensitive to contact-pad capacitance and conductance Y , to determine Z_0 .

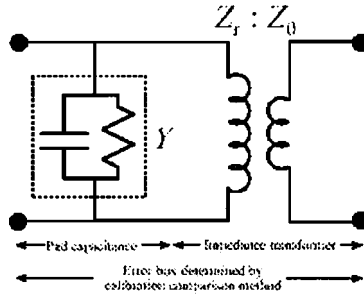


Figure 7 The equivalent circuit model for the contact pads and impedance transformer

Once the frequency propagation constant γ is determined from the TRL calibration, and Z_0 is determined from the calibration comparison method. C , G , L , and R can be determined

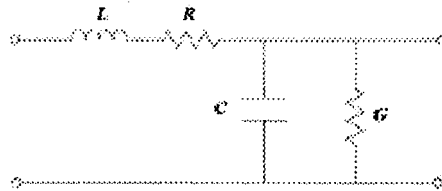


Figure 8. Transmission line equivalent circuit model

by $j\omega C + G = \frac{\gamma}{Z_0}$ and $j\omega L + R = \gamma Z_0$. For a microstrip with a quasi-TEM mode, C and G are related primarily to the properties of the dielectric material incorporated in the transmission line. R and L are primarily related to the metal conductors. With γ and Z_0 accurately measured the properties of the dielectric and the conductors can easily be separated. Finally from the measured dimensions and capacitance, C , the permittivity of the low-k film can be determined using Poisson's equation. Because of the multi layer dielectric configuration of the substrate this will most likely be done with a software package.

2.4

TRL Calibration Standard Design Considerations

The TRL calibration requires a total of twelve measurements to quantify ten unknowns [7]. When building a set of TRL standards the requirements of each of these standards must be satisfied.

The thru (zero length) must have zero loss, $S_{12}=S_{21}=0$, and a phase of 0° . The characteristic impedance Z_0 need not be known. If a non-zero length thru is used the Z_0 of the thru must be the same as the line, or the average of the two is used. Attenuation of thru need not be known. If the thru is used to set the reference plane the phase of electrical length

must be well-known and specified. If a nonzero length thru is set to have a zero delay the reference plane is specified in the middle of the thru, resulting in phase errors during measurements.

In the reflect device the reflection coefficient Γ need not be known, but should optimally have a magnitude of 1.0. The reflection coefficient Γ must be identical at both ports with a known and specified phase to within $\pm 90^\circ$. An error in definition would show up as a 180° error in phase measurement.

The line standard is used to set the reference impedance of the measurement, $S_{12}=S_{21}=0$. The calibration impedance is defined to be the same as Z_0 . The insertion phase of the line must be known and specified within $\pm 90^\circ$, and not be the same as the thru, the difference between the thru and the line must be 20° and $160^\circ \pm n \times 180^\circ$. An approximation of the phase difference is given by $\phi \approx .012 \cdot f \cdot \ell / V_f$. The electrical length ℓ is equal to the length of the line minus the length of the thru, and is calculated with $\ell = \frac{c \cdot V_f}{4 \cdot f_{\text{center}}}$. Where V_f , is the velocity factor $V_f = \frac{1}{\sqrt{\epsilon_{\text{eff}}}}$. The effective dielectric constant ϵ_{eff} can be calculated using appendix D, however there are many software packages available to do this. AppCAD by Agilent Technologies was downloaded for free from their website and used for this task. When the insertion phase nears 0 or $n \times 180^\circ$ the measurement uncertainty will increase greatly. The optimal line length is 90° of the insertion phase relative to the thru at F_m , the frequency at the middle of the frequency span. The usable bandwidth for a single thru/line pair is 8:1,

frequency span: frequency start, and multiple thru/line pairs with identical Z_0 can be used to extend the usable bandwidth. Attenuation of the line need not be known.

Microstrip

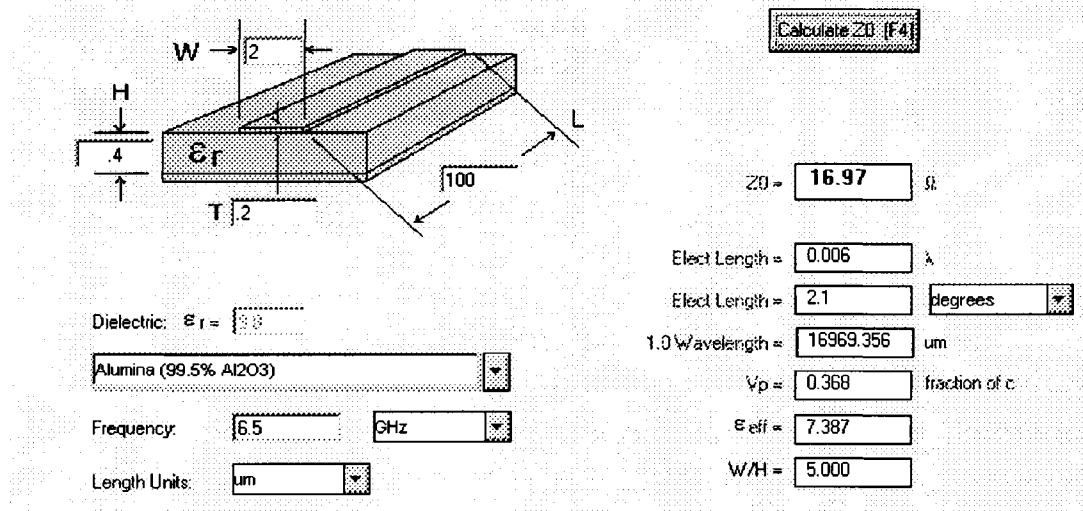


Figure 9. AppCad window used to calculate a thru standard on SiC

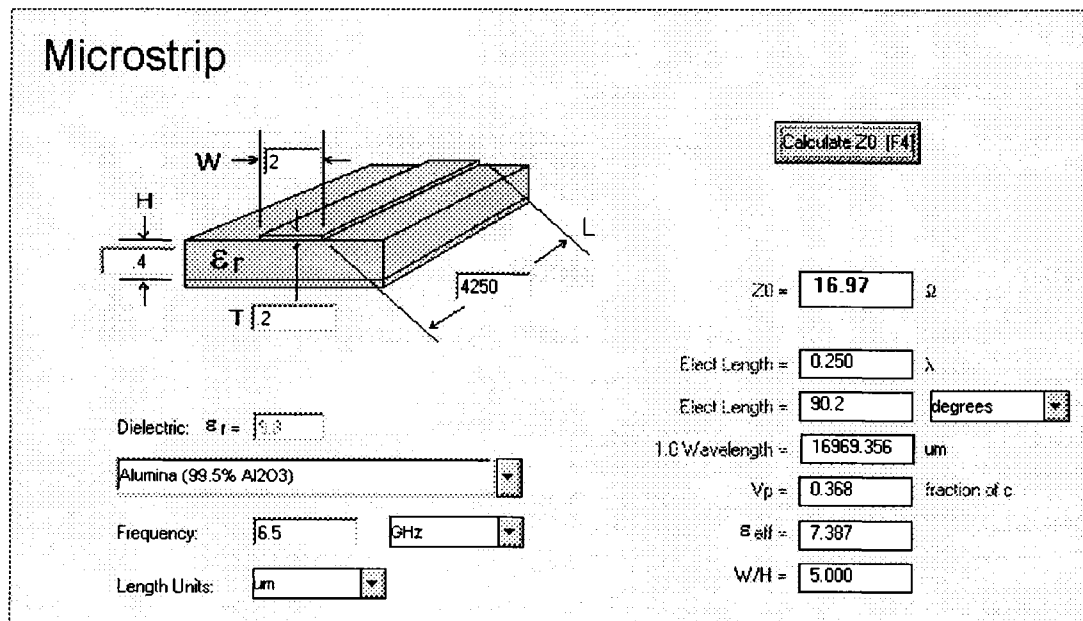


Figure 10. AppCad window for a 4250 micron line standard on SiC

Chapter 3

FABRICATION PROCESS

The fabrication process for the transmission lines and TRL calibration standards used standard laboratory methods for building microelectronic devices. The aluminum films used for masking the substrate during plasma processing, and for the metal lines in the devices, was deposited with DC magnetron sputtering. Argon laser beam lithography was used for creating the photomasks used to create the various aluminum features. The plasma processing was done in a RF magnetron gun using HFC 134a and oxygen gasses. Each of these processes will be detailed in this chapter.

3.1

Basic Outline for the Fabrication Process

The following steps detail the fabrication process required to manufacture the microstrip devices.

1. DC magnetron sputter 2000Å aluminum for a mask of the ground features to be plasma etched.
2. Make photomask of ground lines in the aluminum and wet etch the aluminum mask for the ground features.

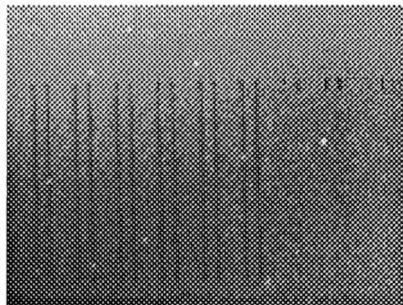


Figure 11. Ground lines etched in aluminum. The lines are all 10 μm wide, and the lines for the line structures are 4250 μm long, and the lines for the thru structure are 300 μm long.

3. Plasma etch the SiC (and low-k) for ground features.

- Strip aluminum mask.

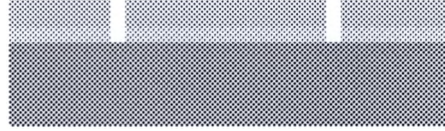


Figure 12. Side view of the sample after plasma etching the trenches for the ground contacts with the substrate. The top layer is the low- k the middle layer is the SiC and the bottom layer is the Si substrate.

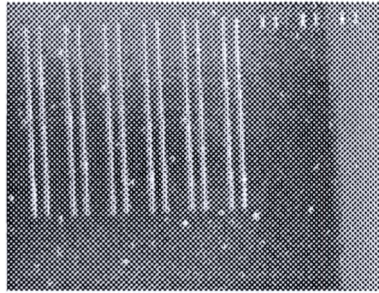


Figure 13. Top View of SiC after plasma etching, and the aluminum mask has been removed

- Photomask for metal ground and microstrip lines and pads.
- Sputter and lift-off aluminum for microstrip line.

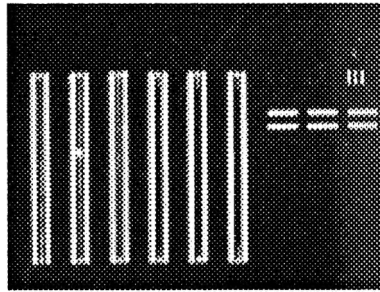


Figure 14. Aluminum Microstrip lines after sputter end lift off. The line width for the microstrip is $2.5\ \mu\text{m}$. the three pairs of horizontal bars below the thru lines are the reflect standards (shorts)

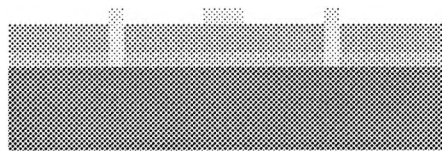


Figure 15. Cross section of microstrip showing the ground returns contacting the substrate, and the signal line is on top of the low-k SiC stack.

3.2

DC Magnetron Sputter Deposition

Aluminum thin films used for the masks and microstrip structures were deposited with Pulsed DC Magnetron sputtering. Magnetron sputtering is a low pressure plasma process. A vacuum chamber is evacuated to remove water and other environmental gasses, and then a sputtering gas is flowed into the chamber at a controlled rate. In this case a toroidal

magnetron gun is used as the plasma source. It is essentially a capacitor with an ultra pure material as one of its plates with a strong magnetic field around it. When the magnetron gun is powered, the electric field it produces highly ionizes the sputtering gas, producing a plasma. The magnetic field is used to contain the plasma in the shape of a toroid above the ultra pure material on the target. Ions in the plasma bombard the target and the collisions sputter the material off the surface, this material will then begin to deposit elsewhere in the chamber. A substrate placed above the magnetron gun will get coated with the target material.

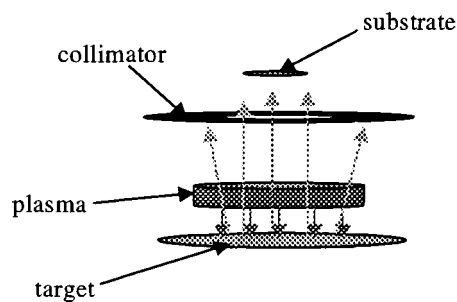


Figure 16. Schematic of magnetron gun

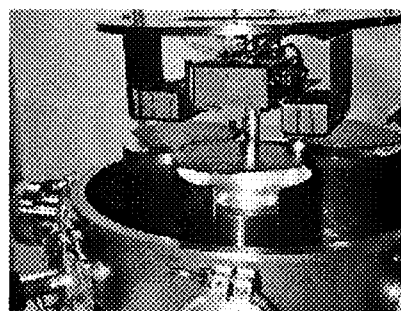


Figure 17. View of magnetron chamber

For this case the chamber was pumped to a base pressure of 4×10^{-7} Torr using a Pfeifer vacuum TC600 Turbo pump in stand by mode (550 Hz). An Argon flow rate of 7.75 sccm (standard cubic centimeters) controlled with a MKS 247C controller and a 10sccm mass flow controller resulting in a pressure of 6 mTorr with the throttle valve fully closed and the turbo pump on stand by. The MDX-1K DC power supply was used with a power of 200 Watts, and was set to Arc Out Mode yielding a deposition rate of 100 Angstroms a second.

The Sparc-le 20 (Small Package Arc Repression Circuit-Low Energy) 20kHz is the core to pulsed DC sputtering, it receives the DC power from the MDX power supply and in Arc Out mode functions as a resonant LC network. During an arc it will discharge and then commutate

off the arc through its reversing action. The ability to quickly clear arcs improves film quality and lessens defects.

3.3

Photolithography

All photolithography was done with the Florod Argon Laser Writer. The photolithography process is a combination of several steps, spinning, baking, exposing, and developing. Each of these steps will be explained in some detail.

3.3.1

Spin

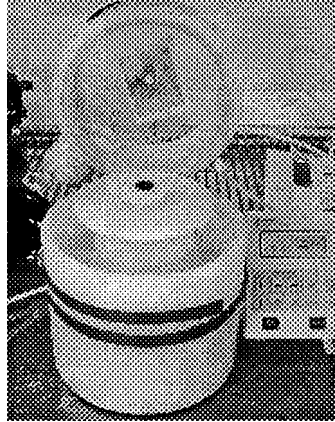


Figure 18. Laurell Technologies Corp. WS-400A-6NPP-LITE spinner used to deposit the photoresist

Spinning is a process used to distribute a material on the surface of a substrate to form a thin film with good uniformity over a range of thicknesses. A Laurell Technologies Corp. WS-400A-6NPP-LITE spinner was used to distribute a film of Shipley AZ 5214-E photoresist. The spinner can be programmed for multiple steps of different acceleration, time and revolutions per minute. For all spins the program B was used. Program B is a single step program with acceleration level 25 (2125 rpm/s), a velocity of 3000 rpm, and a duration of 30 s. This will result in a film of photoresist 1.63 microns thick [9]. The basic procedure for this process step is to drop a few ml of resist on the wafer with a plastic pipette, spin for 30 s at 3000 RPM. Next soft bake the sample for 1 min at 90 °C.

3.3.2

Bake

Three different bakes are used in the process a pre-bake, a soft bake and a post bake. Humidity is a factor for adhesion of the photoresist. The humidity needs to be between 20 to 60 percent, however the humidity is typically higher in San Marcos Texas. To counter this a pre-bake is used; the substrate is placed on a hot plate for 60 s at 110 °C immediately before being placed in the spinner. The soft bake is used after the photoresist is spun on. To soft bake, the substrate is placed in a hotplate at 90 °C for 60 s. Soft baking dries the photoresist by evaporating the solvents. To further help with adhesion and to improve the wet etch profile of the Al mask a post bake is used. The substrate is placed on the hot plate for 120 s at 120 °C up to a few hours before wet etching.

3.3.3

Exposure

The photoresist was exposed with the Laser Writer made by the Florod Corp. model LDS. The laser writer uses a 500 mW Argon Ion laser model 532 filtered to the 460 nm line. It has a system of optics and apertures to produce a small square beam to expose the resist. The APO SL 50X lens was used with an aperture of 40 X 40 was used to achieve a 5 μm beam.

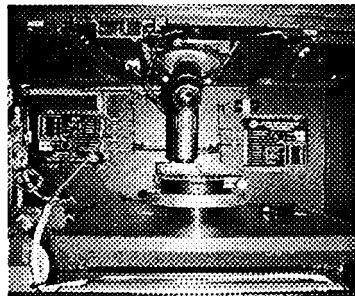


Figure 19. Inside view of laser writer. Samples are placed on the rotation stage below the microscope lens. The stage can be rotated to help align the features for the second lithography.

A computer controls a stepper motor driven stage with an accuracy of $1/40^{\text{th}}$ of a micron in the X and Y direction. An electromechanical shutter is controlled to turn the light on and off in conjunction with moving the stage in order to “write” the programmed features. A script defines the stage acceleration velocity user units (a unit is $1/40^{\text{th}}$ of a micron, so a user unit of 40x will set a distance of 1 equal to a micron) and 0,0 position. It then runs an auto focus

procedure that uses a CCD camera connected to a PROSCAN auto focus controller. The procedure moved the stage to four points on the outer corners of the feature and uses the image contrast on your alignment beam to set the Z height of the lens. The focus controller then linearly interpolates Z during the writing procedure to keep the beam in focus. Once the focus procedure is complete, the script controls the stage and shutter to expose the desired features.

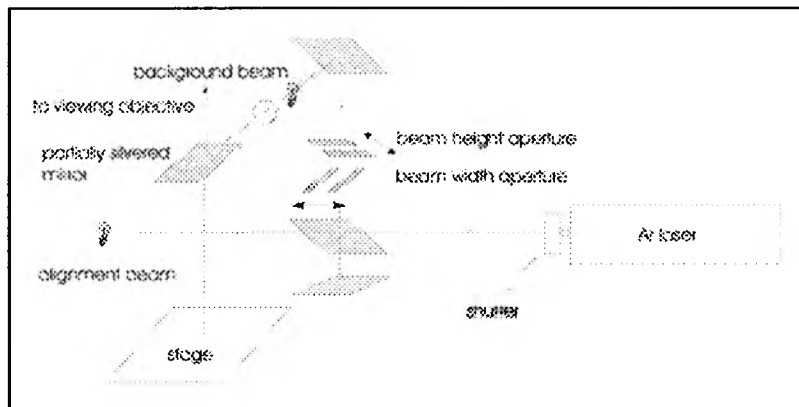


Figure 20. Schematic of laser writer

3.3.4

Develop

After the samples are exposed, they are developed to remove the exposed photoresist and reveal the desired features. The developing procedure uses Shipley AZ 400K developer

diluted 4:1 with DI water. The exposed samples were hung in a 50 ml graduated cylinder with 5ml developer and 20 ml DI water via locking forceps and agitated gently in the solution for 60 s. The sample is then inspected under a 5x microscope and if needed, can be developed for an additional 15 to 30 seconds.

3.4

Wet Etch

After the photoresist masks are made on top of the sputtered aluminum, the next step is to etch through the exposed aluminum to create the aluminum mask of the vias. This was done using Aluminum Etchant Type A ($16 \text{ H}_3\text{PO}_4 : 1 \text{ HNO}_3 : 1 \text{ HAc} : 2 \text{ H}_2\text{O}$)[20]. This wet etch is isotropic in nature so it is important not to over etch the sample as under cutting of the mask will occur. Approximately 15 ml of etchant was placed in a 20 ml beaker and set on a hotplate at 50°C . Samples were set in the etchant and slowly agitated until the exposed areas turned dark gray. Aluminum Etchant Type A has an etch rate of up to 6600 Angstroms/min [20] but this can reduce significantly as etchant gets dirty so detecting the endpoint visually is necessary. Once etching is finished the sample is immediately rinsed with DI water and blown dry with nitrogen gas.

3.5

Strip

When a photoresist layer is no longer needed, a process called stripping removes it. In order to strip the mask, the sample is rinsed in acetone. The acetone removes the photoresist at a rate of > 39 k Angstrom/min [20]. The sample is then rinsed in isopropanol and blown dry with nitrogen gas.

3.6

Plasma Etch

After the photoresist is removed, an aluminum mask remains on the surface of the wafer. The masked wafer is then etched in the magnetron with a plasma consisting of HFC 134a (1,1,1,2-tetrafluoroethane) and O_2 at 20 mTorr to remove the exposed low-k and SiC under layer. In this process the primary mechanism for material removal is F-C and F-Si reactions between fluorine ions and the Si and C atoms, followed by ion sputtering removal. This etch

process should be anisotropic in nature due to the SiC providing carbon, enhancing polymer formation on the sidewalls of the feature. This polymer inhibits sidewall etching and therefore stops undercutting.

Chapter 4

PLASMA ETCH RATE STUDY

A major portion of this research was dedicated to developing a reactive ion plasma etch process in order to etch through the SiC under layer to access the substrate for a ground contact between the substrate and the ground lines. A method was devised using a magnetron gun attached to an RF network as a plasma source and a mixture of tetrafluoroethane or HFC 134a and O₂ as the process gas. Tetrafluoroethane is of interest due to its high fluorine content, and it is readily available. In fact I purchased a can of Genetron 134a at the local automotive parts store. It is also a nontoxic, ozone-friendly gas with a short atmospheric lifetime.

HFC 134a Specs.

-1,1,1,2-tetrafluoroethane 99.5%

-Formula: C₂H₂F₄

-Molecular Weight: 102.03

-CAS Registry Number: 811-97-2

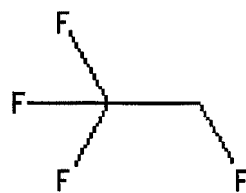


Figure 21 HFC 134a molecule

4.1

Reactive Ion Etching

The material removal in reactive ion plasma etching is a combination of several mechanisms [10]. 1) Sputtering – the physical removal of material by energetic ion bombardment. 2) Chemical plasma etching – neutral radicals produced in the plasma remove material by chemically reacting with the substrate material and producing volatile species. 3) Ion-enhanced chemical etching – energetic ions damage the surface of the substrate enhancing the absorption rate of the etching species. 4) Inhibitor controlled chemical etching – inhibitor layers are removed by ion bombardment allowing the reaction to proceed. Giving an overall etch rate of R [10].

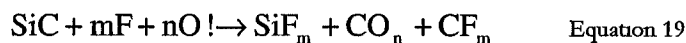
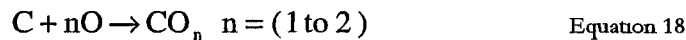
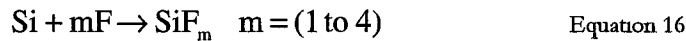
$$R = R_{\text{Sputter}} + R_{\text{Neut}} + R_{\text{IEN}} + R_{\text{ICN}} \quad \text{Equation 14}$$

The effects of the arrival rate of ions and neutrals on the overall etch rate can be explained by expanding the sputter rate equation [11, 12, 13] as follows:

$$R = F_I \varphi_s + F_N (1 - a\alpha - \beta) \varphi_N + F_N \alpha \varphi_N^* + F_N \beta \varphi^* N^* \quad \text{Equation 15}$$

Where F_I is the ion flux (ions/cm² s), F_N is the flux of neutral particles, φ_s is the sputtering efficiency (cm³/ion), φ_N is the chemical etch rate efficiency of neutral species (cm³/neutral),

ϕ_N^* and ϕ^*N^* are the chemical etch rate efficiencies of neutral species on the fraction α of the surface which has been sensitized, ion bombarded, and on the surface fraction β covered by an etch inhibitor. This model explains the association between the neutral radicals and ion plasma species involved in the etching process. The ion flux increases the sensitized surface fraction, and negatively affects the inhibitor covered fraction, enhancing the chemical neutral etch rate. For SiC etching in mixtures of fluorinated gases and oxygen, the most probable chemical reactions for the removal of Si and C atoms are given in equations 16-18 [14], giving the combined chemical reaction, equation 19, for the removal of SiC molecules. It should be noted that this model doesn't consider the other reaction compounds, such as COF₂. [15]



An anisotropic etching profile was obtained for SiC in SF₆/O₂ mixtures, which is not the case of the normally undercut etching profile for Si [16, 17]. The reason is due to SiC itself providing carbon, which promotes polymer formation, preventing the sidewall from being etched. However, there were no fluorinated gases investigated by [10] which produced an undercut profile during SiC etching. Therefore we can assume HFC 134a will also produce an anisotropic etch, however we have not verified this. In addition to the indirect roles of oxygen

in the gas phase reaction, oxygen also participates by directly removing C atoms in SiC through the reaction given in Equation 18. Carbon can be etched in either pure fluorine containing plasma (equation carbon-fluorine, C-F, or carbon-oxygen, C-O, reactions [10]). At low O₂ percentage, it has been suggested [18] that carbon is preferentially removed through the formation of CF_m (Equation 16) rather than as the C-F reaction [10]. Along with the purely chemical plasma etching process, the effect of the energetic ion flux needs to be considered. The ion bombardment breaks the surface Si-C bond (4.52 eV), which enhances the chemical reaction efficiency, and removal of non-volatile surface species. This enables the chemical reaction to proceed, including providing sufficient energy to break the strong C-C bonding (6.27 eV) that could exist in the C-rich layer [10]. This combination of effects have led to a two regime model for the effect of DC bias on the etch rate of polycrystalline SiC [14]: a) at low dc bias conditions, the low energy and effectiveness of the ion flux is the dominant mechanism; b) at sufficiently high values of the dc bias, the ion energy is high enough to no longer limit the process and the etch rate is determined by the removal efficiency of the chemical reaction [10].

There was not any etch rate data available for SiC with HFC 134a. Therefore this process required an etch rate study in order to determine the right mixture of HFC 134a and O₂, and the respective etch rate. A constant flow of HFC 134a was investigated as compared to various oxygen flow rates.

4.2

Experimental Setup

For this study the samples consisted of approximately 350nm of SiC on top of a Si substrate. The thickness of the SiC film was measured optically with a Filmetrics system, this measurement correlated to profilometer measurements taken after etching. 1000nm of Aluminum was sputtered on to the substrates and masks were made using the method described in chapter 3. The masks were in the shape of four 100 μm squares spaced 250 μm apart, and all with a 10 μm x 500 μm line protruding from the center of one face. The etch samples were placed on top of a Si target in the magnetron gun, and arranged so that the highest plasma density was in the area of the mask features. The HFC 134a flow rate was fixed at 11sccm and the O₂ flow was studied at 4, 6, 7.33, 9, and 11 sccm, resulting in a process pressure around 20 mTorr. All etches were done at 50 Watts RF (0.6 Watts/cm²). The substrates were allowed to self-bias during etching and the bias voltage was recorded by the computer. The computer also controlled the RF network that powered the magnetron guns.

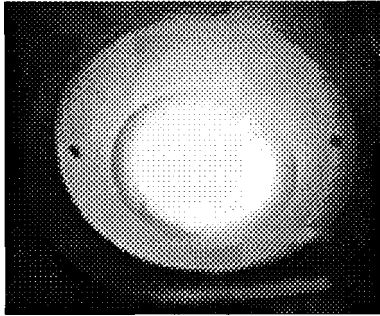


Figure 23. Samples being etched in the magnetron gun by a plasma

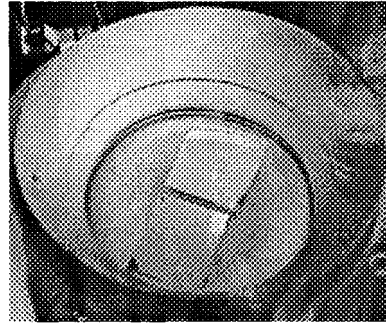


Figure 22 Two samples on top of an Si target in the magnetron gun before etching.

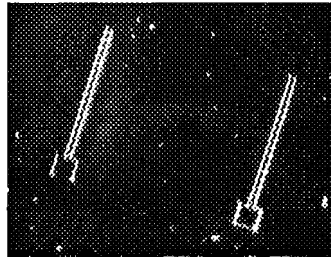


Figure 24. Photo of features etched in SiC after the aluminum mask has been removed

The RF network that powered the magnetron consisted of an Advanced Energy RFX600A 600 Watt RF power supply, and an Advanced Energy ATX-600 impedance-matching network. The power supply generates an RF power signal at 13.56 MHz, and is designed to power a 50 Ω non-reactive load. Because the basic characteristics of a plasma can be electrically represented as a diode, a resistor, and a capacitor in parallel, it has a reactive impedance that is related to the chamber, the ion composition and other chamber conditions. The diode effects arise from the fact that the much lighter electrons can move much faster

than the ions. In order to provide the non-reactive $50\ \Omega$ load, a matching network is connected in series between the power supply and the magnetron gun.

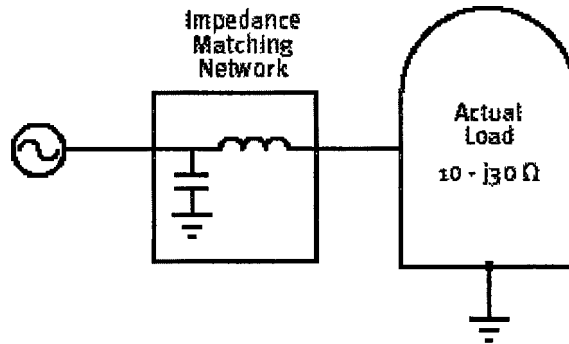


Figure 25 Schematic of an impedance matching network attached to the magnetron chamber

The function of an impedance-matching network is to transform the resistive and capacitive characteristics of the plasma to $50\ \Omega$. The impedance-matching network is constructed of a combination of capacitors, resistors, and inductors. There are two active components in the matching network, a forward power and a reflected power capacitor. These capacitors are variable open-air capacitors that are controlled either manually or by the ATX-600 controller to tune the system to the required $50\ \Omega$ load, thus matching the load impedance to the AC generator's impedance.

Because the films being etched were so thin and initial etch rates were high a method of controlling the etching times to a high degree of accuracy was needed; Simply turning on and off the power supply with a stop watch in hand was not sufficient. A system was developed for computer automating the power supply with the use of a software package called Labview, and a PCI-6023E data acquisition (DAQ) card both by National Instruments. Labview is a Microsoft Windows based graphical programming package that gives the programmer the ability to easily design logic circuits and manipulate both analog and digital, in and out signals,

with the use of a DAQ card. This provides the ability to interface with the pin-out on the RFX600A power supply. Allowing not only to accurately control the timing of the power, but to set all of the device parameters and to record the forward power and bias voltages at 0.1 s intervals to extract even more information about the etches.

The aluminum masks for etching, and the microstrip structures were sputtered to 200 nm in thickness. All sputtering was done at room temperature. All substrates were first cleaned with an acetone bath followed by a wipe with an isopropanol wetted Kimwipe and then dried with nitrogen gas. After film deposition masks were placed on samples and a trench was etched in the aluminum. to calculate etch rate.

4.3

Etch Rate Results

The etch rates were determined by etching over different time intervals, removing the aluminum masks, and measuring the feature depth with a Tencor Alpha Step 500 Stylus Profilometer. Further information about the etch profile and roughness was collected with an Atomic Force Microscope. As depicted in the following graphs the highest etch rate of 9.2 nm/s was achieved at a mixture of 11 sccm HFC 134a and 6.0 sccm O₂. AFM imaging shows a very flat RMS roughness of 11.8 Angstroms at the highest etch rates. Etch profile shows high aspect ratio should be achievable.

Etch Depth (Angstroms)					
Oxygen Flow Rate (sccm)					
Time (s)	4	6	7	9	11
5		474	586		
		494	594		
		501	593		
		496	576		
avg		491	587		
10		881	982		
		966	1083		
		941	1052		
		914	1157		
avg		926	1069		
15		1398	1315		1212
		1414	1411		1209
		1499	1431		1069
		1398	1514		1031
avg		1427	1418		1130
25	899	2518	2260	1954	1919
	761	2584	2539	1967	1930
	847	2548	2436	1833	2019
	746	2347	2335	2101	1988
avg	813	2499	2393	1964	1964
35	1524	3359	3120	2335	2376
	1516	3120	3450	2400	2490
	1331	3256	3321	2550	2400
	1338	3278	3107	2778	2364
avg	1427	3253	3250	2516	2408
45	2216	3689	3313	3550	2515
	2090	3663	3501	3462	2774
	2290	3940	3553	3465	2736
	2500	3868	3530		2861
avg	2274	3790	3474	3492	2722
60	2663		3962	3735	3596
	2540		4000	3883	3735
	2693		4037	3923	3883
	2729		3850		3923
avg	2656		3962	3847	3784

Table 2 SiC etch depth in angstroms over time at different oxygen concentrations

Average SiC Etch Rate (/Second)					
Oxygen Flow (sccm)					
Seconds	4	6	7.33	9	11
25	33	100	96	79	79
35	41	93	93	72	69
45	51	84	77	78	60
60	44		66	64	63
avg	42	92	83	73	68

Table 3 Average SiC Etch Rate at various oxygen concentrations

Etch Rates of Various Fluorinated Gasses (Å/Min)				
	HFC 134a / O ₂	CF ₄ / O ₂	CHF ₃ / O ₂	CBrF ₃ / O ₂
SiC	5520	525	675	570
Si	2760	1050	465	225
Selectivity (SiC/Si)	2.0	0.5	1.5	2.5

Table 4 Etch rates of various fluorinated gasses (CF₄, CHF₃, and CBrF₃ are from reference 10. The original values were given at 0.4 W/m², they were linearly interpolated to 0.6 W/m² for comparison to HFC 134a studies done in our equipment)

Si and Al Etch Rate (ER)								
O2 Flow (sccm)	Time Sec	Al Depth (Å)	Post etch Depth(Å)	Si Depth (Å)	post - Si (Å)	Al ER (Å /s)	Si ER (Å/s)	Al ER (Å/s)
11	120	8698	10390	3674	6716	1982	30.62	16.52
		8689	8974	3787	5187	3502	31.56	29.18
		8695	8273	3797	4476	4219	31.64	35.16
		8620	8726	4367	4359	4261	36.39	35.51
Avg		8675.5	9090.75	3906.25	5184.5	3491	32.55	29.09
STDEV		4.58	1078.44	68.31	1084.58	1064.59	2.60	8.87
9	60	10330	14490	2992	11498	-1168	49.87	-19.47
		10390	12630	2771	9859	531	46.18	8.85
		10710	13100	2616	10484	226	43.60	3.77
		10750	12400	2616	9784	966	43.60	16.10
Avg		10545	13155	2748.75	10406.25	138.75	45.81	2.31
STDEV		215.64	936.46	177.87	792.60	922.57	2.96	15.38
7.33	112	8228	6483	5030	1453	6775	44.91	60.49
		8096	15221	5352	9869	-1773	47.79	-15.83
		7992	9292.9	5563	3729.9	4262.1	49.67	38.05
		7834	14149	5183	8966	-1132	46.28	-10.11
Avg		8037.50	11286.48	5282.00	6004.48	2033.03	47.16	18.15
STDEV		166.53	4111.86	228.89	4065.91	4161.66	2.04	37.16
6	126	12070	17220	7787	9433	2637	61.80	20.93
		12020	18960	7768	11192	828	61.65	6.57
		12060	15310	7136	8174	3886	56.63	30.84
		12070	15350	6968	8382	3688	55.30	29.27
Avg		12055	16710	7414.75	9295.25	2759.75	58.85	21.90
STDEV		23.80	1744.73	424.52	1379.36	1399.62	3.37	11.11
4	240	9021	13606	6373	7233	1788	26.55	7.45
		8942	13977	5942	8035	907	24.76	3.78
		8964	12901	6155	6746	2218	25.65	9.24
		8998	12328	6123	6205	2793	25.51	11.64
Avg		8981.3	13203	6148.25	7054.75	1926.5	25.62	8.03
STDEV		35.11	734.46	176.76	776.76	794.64	0.74	3.31

Table 5 Si and Al Etch Rates at various oxygen concentrations

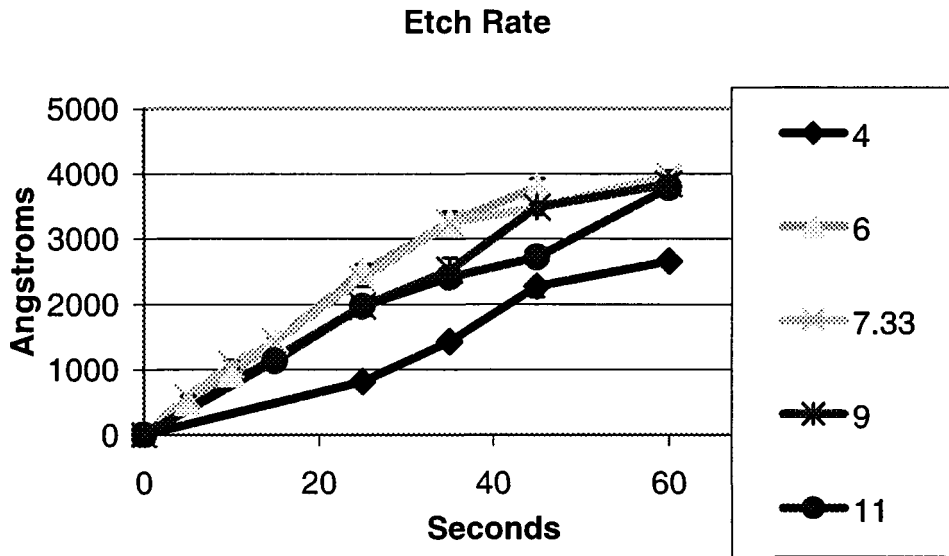


Figure 26. SiC etch rates over time at different oxygen flow

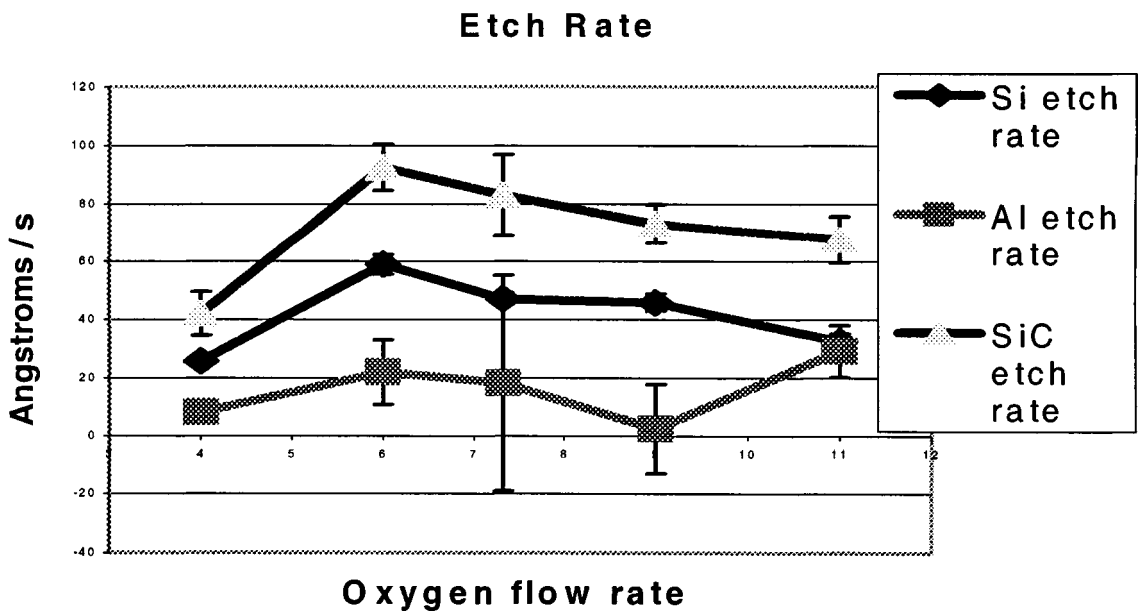


Figure 27. Graph of etch rate vs. oxygen flow for Si, SiC, and Al.

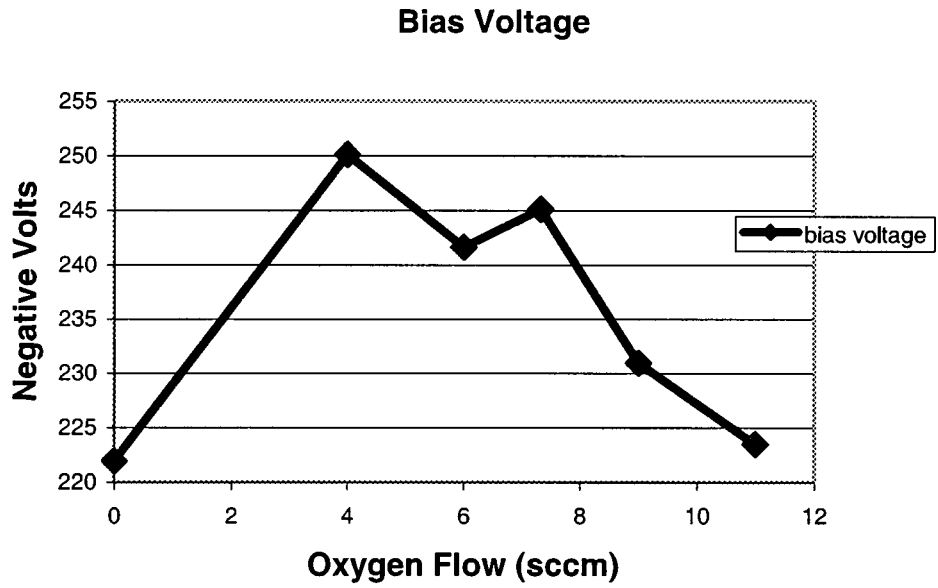


Figure 28. Graph of bias voltage vs. oxygen flow

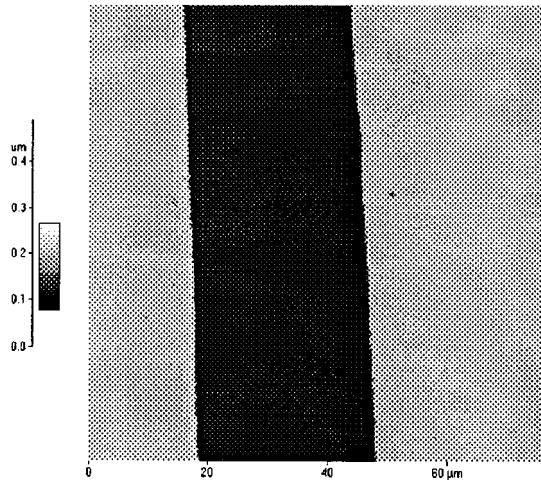


Figure 29. AFM image of trench etched in SiC

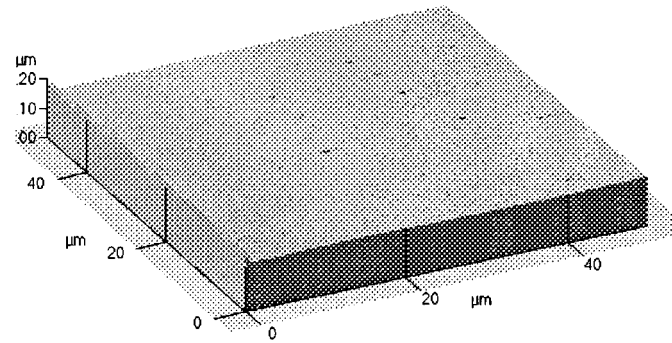


Figure 30. AFM image of the bottom of an etched SiC feature, the RMS roughness is 11.8 Å

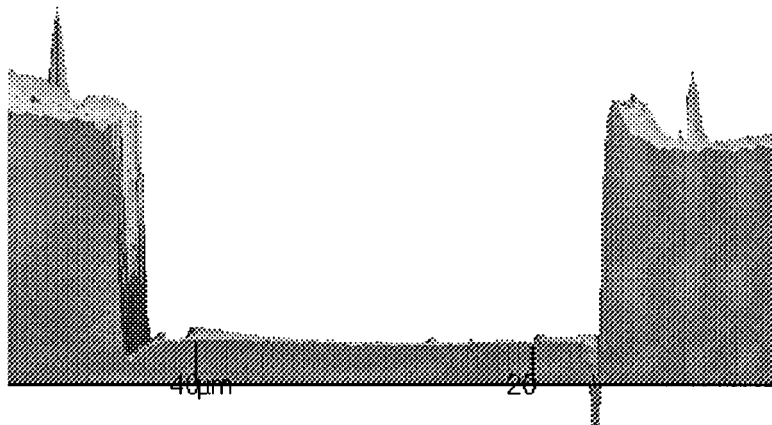


Figure 31. AFM image of cross-section of the etched trench in SiC form Figure 29.

4.4

Etch Study Conclusion

HFC 134a is a viable alternative to more common industrially used etch gases. SiC etch rates as high as 92 Å/s at 0.6 W/m² were achieved, with a 2:1 selectivity with Si and a 4:1 selectivity with Al. Etch rates are much higher compared to other fluorinated compounds used in previous studies (CF₄, CF₃, etc) [10]. Etch rates were highest at a relatively high O₂ content as compared to single carbon gases which have higher etch rates at low O₂ content [10]. This can be explained by the extra carbon provided by the HFC 134a being removed by the C-O reaction allowing the SiC to be etched with the more efficient fluorine reactions. Si and Al selectivity were also seen to be in line with previously studied gases [10].

Chapter 5

MICROWAVE ELECTRICAL MEASUREMENTS

The electrical characterization of the microstrip transmission lines is done on a Cascade Microtech microwave probe station in conjunction with an Agilent 8719ES network analyzer. The network analyzer is first calibrated with a two-tier multi-line TRL using the NIST MultiCal software. The scattering parameters of the test microstrips are measured, and the Z_0 is determined using the calibration comparison method in the NIST MultiCal program.

5.1

Cascade Microwave Probe Station

The microwave probe station has two planarizable micropositioning arms that accurately position the probes to contact the microstrip pads as depicted in figure 29. The probes are Air Coplanar™ GSG microprobes with a 150 μm center-to-center spacing (pitch). Each port of the Agilent network analyzer is connected to a probe with a coaxial cable to allow accurate

measurement of the s-parameters at a distance from the device. The DUT is placed on the stage of the probe station and held in place with a vacuum chuck. A microscope is positioned above the probes to facilitate accurate placement of the probes on the microstrip pads.

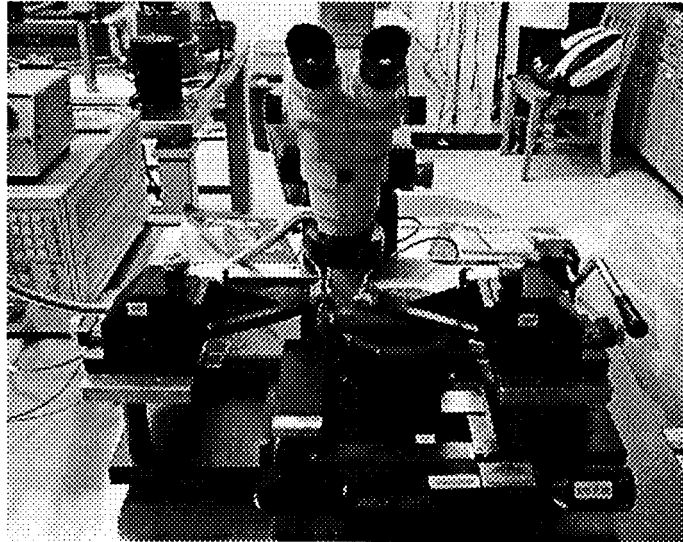


Figure 32. Cascade Microtech microwave probe station

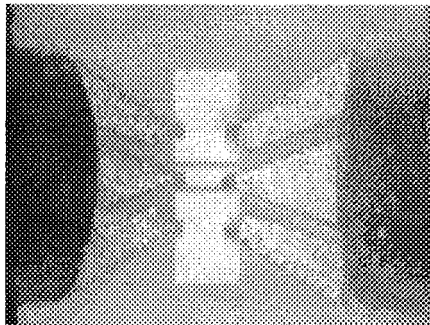


Figure 33 Picture of the open air coplanar probe contacting thru standard. The probe pitch is $150\mu\text{m}$.

5.2

Agilent 8719ES network analyzer

The Agilent 8719ES VNA can measure the s-parameters of the DUT from .05 to 13.5 GHz. It interfaces with a PC using a GPIB 488 standard. Data can be recorded in the s2p TOUCHSTONE format using an Excel plug-in provided by Agilent. The file extension can be changed to sp2 and the files are then compatible with the NIST MultiCal software.

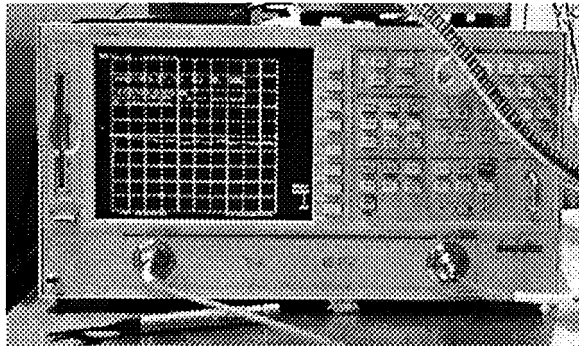


Figure 34. Agilent 8719ES VNA

5.3

NIST MultiCal

The NIST/Industrial Measurement Consortium developed MultiCal on-wafer measurement software implementing the multiline TRL calibration, LRM with imperfect standards, off-wafer CPW calibrations, calibrations for lossy lines, and the calibration comparison method for accuracy assessment. MultiCal was written for the HP9000 series, but this program can be run on a windows system under a Rocky Mountain Basic command interpreter, HT Basic by Trans Era Corp. (<http://htbasic.com>) has a demo version available for download. The MultiCal[®] software suite also determines the complex frequency-dependent characteristic impedance of the transmission lines used in the calibration and allows the user to set the calibration reference impedance to the characteristic impedance of the line, to 50Ω, or to any other real value.

The menu-driven software calibrates VNA's using the de-embedding algorithms developed at NIST. The basic de-embedding algorithm used in MultiCal is the multiline TRL algorithm. If more standards are available than the minimum needed, the algorithm automatically weighs the results for maximum accuracy. The MultiCal TRL algorithm also optimally measures the propagation constant of the calibration lines. MultiCal can determine and reset the calibration reference impedance using the calibration comparison method for

lossy and dispersive substrates. MultiCal also supports an off wafer calibration method [19] that can correct for differences in substrate dielectric constants. The software supports both one-tier and two-tier de-embedding. The two-tier algorithms can be used to electrically characterize probe heads, and to implement the calibration comparison method. After de-embedding, MultiCal can plot and analyze various data including propagation constant and impedance parameters.

<http://www.boulder.nist.gov/div813/rfelec/micro/dylan/software.html> is the URL to download the software. The password for MultiCal is "multical". The password for the other software on the web page is "mmic". Dylan Williams [dylan@boulder.nist.gov] will answer any questions about the software.

Chapter 6

CONCLUSIONS

The fabrication of microstrip transmission lines has been successfully accomplished. This process included a new method of reactive ion etching SiC utilizing an HFC 134a and O₂ plasma, DC magnetron sputtering, argon laser beam lithography, as well as several other common process techniques. A method for measuring and characterizing the microwave electrical properties of the transmission lines using a vector network analyzer and a microwave probe station using the calibration comparison method has also been developed.

6.1

Etch study

The SiC etch study involved a new method of reactive ion etching silicon carbide in a HFC 134a and oxygen plasma. The process achieved an etch rate about ten times higher than

previously reported etch studies while still achieving a high selectivity with Si and Al. Some further investigations might be the role of argon at various flow rates toward the etch characteristics selectivities, as well as the etch rate of SiO₂.

6.2

Microstrip Transmission Lines

At this point microstrip structures have been successfully designed and fabricated. However there are still some problems in the measurement and characterization of them. Microwave measurements are very touchy and probe placement and alignment are critical. There are also some issues with getting the NIST software to function properly. The software is not directly compatible with the VNA, and measurements have to be taken manually with the Agilent Excel plug in as .S2P files and then by changing the file extension to .SP2 they can then be entered in to the NIST software.

After the de-embedding the plots look very noisy as can be seen in the graph. One possible reason for the noise is if the aluminum is forming an oxide during sputtering. For an order of magnitude assessment the measured resistance and the calculated resistance for a wire of the line's dimensions were compared. The measured value was about 75 Ω higher. This difference may be explained by aluminum oxide formation, however the difference is not as significant as would be expected for a completely oxidized line. Some of the difference could

arise from a bad probe contact, yielding a high contact resistance. An AFM image of the line showed small regions of lessened cross-sectional area. These areas would increase the line's resistance; this along with contact resistance could account for the discrepancy.

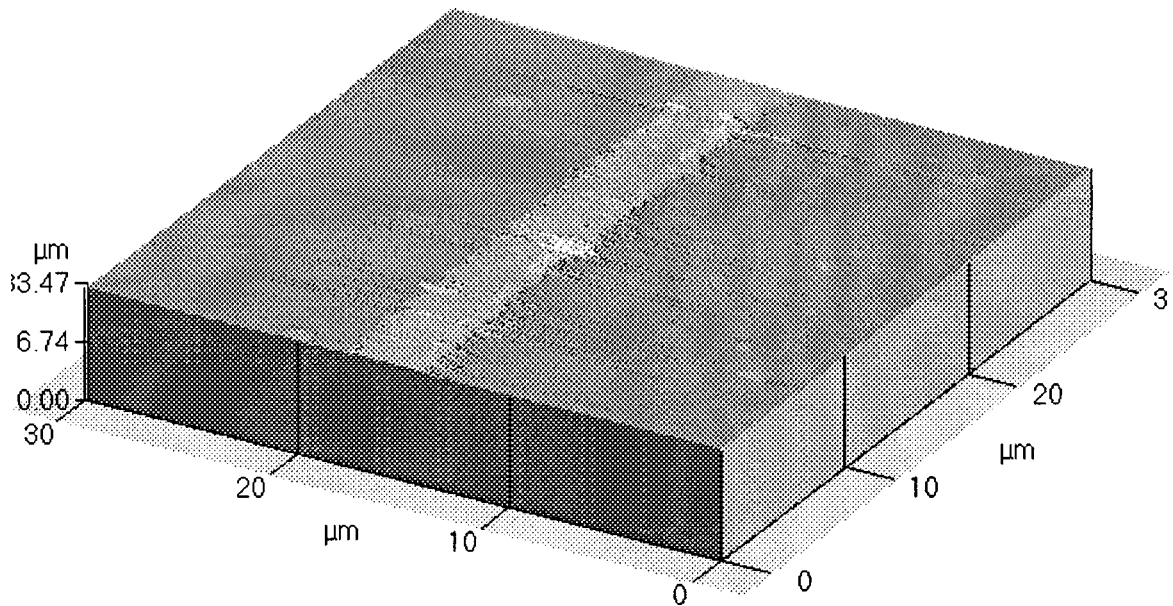


Figure 35. AFM image of aluminum microstrip line on SiC the line is 2500 Å tall and 3.5 μm wide

For better measurements, some work needs to be devoted to improving both the microstrip uniformity, and the probe placement and contacts.

DC Resistance and Capacitance of MS lines			
	CVD	SiC	TRL standard Line 5
Measured Resistance (Ω/cm)	306.4	308.6	12.3
Calculated Resistance (Ω/cm)	224.7	224.7	2.15
Capacitance (pF/cm)	10.6	11.8	10.3

Table 6. DC resistance and capacitance of microstrip lines

APENDIX A

OUTLINE OF FABRICATION PROCESS

1. Preclean samples in acetone and then isopropanol and blow dry with nitrogen.
2. Sputter 3000 angstroms aluminum for mask in magnetron.
3. Spin on photoresist.
4. Photolithography with appropriate file
 - a. 3ms.txt for 3 sets of TRL ground lines.
5. Develop and inspect for proper exposure with 10x microscope.
6. Al wet etch for 45s or until feature visually turns gray.
7. Strip mask with acetone then wash in isopropanol and blow dry.
8. Plasma etch 55 seconds in magnetron.
9. Strip Al mask with Al etch, clean, dry and inspect.
10. Spin on photoresist.
11. Photolithography
 - a. Align.

b. Run appropriate file.

12. Lift off, and inspect.

APPENDIX B

Procedures

Spin Procedure.

1. Place sample in center of chuck and push vacuum button.
2. Dispense approximately 3ml of photoresist with plastic pipet on the center of sample and close lid.
3. Select spinner program B, and press start.
4. Once program is finished open lid and press vacuum.
5. Remove sample and soft bake on the hot plate at 90°C for 60s.

Laser writer Procedure.

Note: The Laser Beam Writer has three light sources. The laser power can be regulated on the remote control box (brown panel with laser enable key). The system also has two halogen lamps. Their intensity can be regulated by two potentiometers on the right side of the microscope. Potentiometer A will regulate the background illumination of the sample so that the sample can be observed through the optical microscope. Potentiometer B regulates the intensity of the light-beam that runs parallel with the laser-beam (alignment

beam). Both the laser beam and this halogen beam B are projected on a variable aperture in the back of the LBW. The microscope images this aperture on the sample. Two knobs that are situated just behind the oculars can be used to modify the width and height of the slit and thus the spot size on the sample.

1. Switch on the computer, switch on the system power, then switch on the laser power. Put the laser in stand-by mode. Push the decrease switch on the remote control panel for 30 seconds, and leave at least one door to the stage housing open.
2. Switch on the laser by rotating the laser-enable key clockwise (past ON). After approximately 40 seconds several clicks can be heard. The argon laser should start.
3. Set the remote control box of the laser to optical control mode.
4. Set the remote control box to "OPERATE".
5. Increase the laser intensity to 90mW.
6. Choose the 50X objective.
7. Set the stutters both to 40.
8. Press F5 and enter "laseroff.txt" at the command prompt to close the shutter.
9. Turn potentiometer A and B clockwise.
10. Place the sample on the XY-stage under the aperture so the red alignment beam, which appears as a small red dot, is near the center of the sample.

11. Turn potentiometer A counterclockwise.
12. Close all doors.
13. Press F5 and run the appropriate file.
14. To switch off the laser system decrease the power to 50 mW, switch to stand-by mode, and turn The laser-enable key on the remote control counter-clockwise to OFF. WAIT for at least 15 minutes before switching off the laser power and the system power switches on the LBW. If you switch off the laser (from the remote control panel), it will not be possible to switch it on again during the same day.

Develop procedure.

1. Mix 5ml AZ 400K developer and 20ml DI water in a 50ml graduated cylinder.
2. Using the blue locking forceps hold the sample in the solution and gently rotate it approximately 1 RPM for 60s.
3. Rinse with DI water and blow dry with nitrogen.
4. Inspect with 10x microscope and develop for another 15 to 30s if needed.

Magnetron procedure.

1. Pump out.
 - a. Remove any debris on the bell jar flange and gasket.

- b. Bring the bell jar in contact with the flange on the well and hold it ensuring that the gasket is centered on the flange.
 - c. Press the button with the circle with a line in the middle of it in the lower left corner of the DCU (located in the center on the magnetron control panel).
 - d. Wait until you have reached the desired base pressure as displayed on the cold cathode gauge.
 2. Turn off the cold cathode gauge.
 3. Open the valve on the right of the chamber correlating to the Mass Flow Controller (MFC) connected to the sputtering gas you are using.
 4. Turn on the Model 247C 4-channel read out on the rack.
 - a. Turn the display channel dial to the channel number for your MFC.
 - b. Set the right toggle switch for the MFC channel to flow.
 - c. Hold the left toggle switch up to SET PT. and adjust the display to the desired flow with the screw just next to the switch.
 - d. Turn the channel for your MFC on with the toggle switch on the 247, a green LED above the switch should illuminate.
 5. Close the throttle valve with the rocker switch on the right on the magnetron panel, red light should illuminate.

6. Move the shutter with the rotators on the side of the base plate to cover the magnetron gun being used.
7. Turn on the appropriate power supply for the gun you are using with the switch on the back and then the switch on the front Note: if you are using the RF power supply go to RF Power supply instructions.
8. Set the display in the power supply to set point power
9. Set the regulation to power.
10. Turn the level knob to the desired power.
11. Press the start or output on button on the power supply (the gun should light)
12. Wait a few minutes to clean the target.
13. Rotate the substrate above the gun with the rotator.
14. Open the shutter using a stopwatch to time the deposition; them close the shutter when time is up.
15. When finished sputtering press stop or output off on the power supply.
16. Open the throttle valve with the rocker switch.
17. Open the chamber

- a. Press the button with the circle with a line in the middle of it in the lower left corner of the DCU (located in the center on the magnetron control panel).
- b. Open the valve on top nitrogen bottle, and after the regulator.
- c. When you hear the vent solenoid open and nitrogen begin to flow turn off the MFC channel on the 247C and close the sputter gas valve to the right of the chamber.
- d. Turn off the 247C.
- e. When the pressure is at 760 Torr the chamber will open.

18. After samples are removed pump out the chamber.

Lift Off Procedure

1. Sonicate the sample in acetone by holding it with the blue locking forceps with the aluminum side facing down.
2. When all the unwanted aluminum is loose lift the sample out of the bath while spraying loose the aluminum on the surface.
3. Rinse with isopropanol and blow dry.

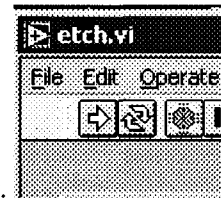
Anneal Procedure

1. Open the nitrogen valve set the regulator to 10 PSI.

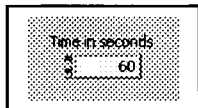
2. Place both end caps on the furnace tube.
3. Place the end of plastic exhaust hose from left the end cap in a beaker full of water.
4. Adjust the needle valve for a slow flow of bubbles in the beaker.
5. Set the furnace to setting 2 (temp should stabilize at 400°C).
6. Place the sample in the sample boat.
7. Wearing the welding gloves remove the exhaust end cap and slide the boat in the furnace tube.
8. Slide the boat to the center of the tube with the glass rod, and replace the end cap.
9. Wait four hours.
10. Wearing the welding gloves remove end cap and remove the boat with the glass rod.
11. Turn the furnace off, and shut the nitrogen valve.

RF Power Supply Procedure

1. Turn on the power switch on the back of the RFX600A power supply.
2. Turn on the ATX-600 with the power button on the front.
3. Double click the etch.vi icon on the desktop of the pc.



4. Click on the arrow button in the upper left corner of the window.



5. Set the sputter time in seconds (default is 60s).
6. Press the RF enable button
7. Set the power level (default is 50 watts)
8. To save bias data
 - a. Press the save bias data button
 - b. Enter a file name for the bias data
9. Flow 11 sccm 134a and 6.0 sccm Oxygen with the mass flow controller
10. Close the throttle valve (pressure should reach ~ 20 mTorr)
11. Switch the RFX 600 power supply to standby
12. Press the start button.

APPENDIX C

LASER WRITER CODE

FILE NAME: MS.TXT

This file draws a microstrip with a 4250 micron line

```
AX LP0 /X
AY LP0 ~ad,25,32,16,4
#1 50000 0
AX UF AY MR-4290 GO
AY UF ID
/Y
AX UU40 ~ad,25,32,16,4
AY UU40 #2 50000 50000
AX MR-350 GO
AX AC50000 ID
AY AC50000 /X
AX VL600 ~ad,25,32,16,4
AY VL600 #3 0 50000
AY MR4290 GO
ID
*****CALIBRATE /Y
~ad,25,32,16,4
*Move in negative X direction #4 0 0
AX MR350 GO #5 0 0
ID
```

*****LEFT GROUND

AX LP0

AY LP0

AX UF

AY UF

AX UU40

AY UU40

AX AC50000

AY AC50000

AX VL200

AY VL200

*****50 UM PAD 50X 40*40

AX UF

AY UF

AX UU40

AY UU40

AX AC50000

AY AC50000

AX VL300

AY VL300

AA MR3,-3; GD

ID /XY

AA

AN0,0

CX

AX MR39; GD

ID /X

AY MR-4; GD

ID /Y

AX MR-39; GD

ID /X

AY MR-4; GD

ID /Y

AX MR39; GD

ID /X

AY MR-4; GD

ID /Y

AX MR-39; GD

ID /X

AY MR-4; GD

ID /Y

AX MR39; GD

ID /X

AY MR-4; GD

ID /Y

AX MR-39; GD

ID /X

AY MR-4; GD

ID /Y

AX MR39; GD

ID /X

AY MR-4; GD

ID /Y

AX MR-39; GD
ID /X
AY MR-4; GD
ID /Y

AX MR39; GD
ID /X
AY MR-4; GD
ID /Y

AX MR-39; GD
ID /X
AY MR-4; GD
ID /Y

AX MR39; GD
ID /X

AA
AF0,0
CX

AA MR3,-3; GD
ID /XY

AA
AN0,0
CX

AX MR-45; GD
ID /X
AY MR45; GD
ID /Y
AX MR45; GD

ID /X
AY MR-45; GD
ID /Y

AA
AF0,0
CX

*****SIGNAL LINE

AX MR-13; GD
ID /X

AX AC50000
AY AC50000
AX VL200
AY VL200

AA
AN0,0
CX

AY MR-4250; GD
ID /Y

AX MR-5; GD
ID /X

AY MR4260; GD
ID /Y

AX MR-5; GD
ID /X

AY MR-4260; GD
ID /Y

AX MR-5; GD
ID /X

AY MR4260; GD
ID /Y

AA
AF0,0
CX

!XYZ

*****MOVE BOTTOM

CENTER
AA MA0,-4290; GD
ID /XY

!xyz

*****50 UM PAD 50X 40*40

AX AC50000
AY AC50000
AX VL300
AY VL300

AA
AN0,0
CX

AX MR39; GD
ID /X
AY MR-4; GD
ID /Y

AX MR-39; GD

ID /X
AY MR-4; GD
ID /Y

AX MR39; GD
ID /X
AY MR-4; GD
ID /Y

AX MR-39; GD
ID /X
AY MR-4; GD
ID /Y

AX MR39; GD
ID /X
AY MR-4; GD
ID /Y

AX MR-39; GD
ID /X
AY MR-4; GD
ID /Y

AX MR39; GD
ID /X
AY MR-4; GD
ID /Y

AX MR-39; GD
ID /X
AY MR-4; GD
ID /Y

AX MR39; GD
ID /X

AY MR-4; GD
ID /Y

AX MR-39; GD
ID /X
AY MR-4; GD
ID /Y

AX MR39; GD
ID /X

AA
AF0,0
CX

AA MR3,3; GD
ID /XY

AA
AN0,0
CX

AX MR-45; GD
ID /X
AY MR45; GD
ID /Y
AX MR45; GD
ID /X
AY MR-45; GD
ID /Y

AA
AF0,0
CX

*****sig pads
AA MA150,0; GD

ID /XY

*****50 UM PAD 50X 40*40

AX UF
AY UF

AX UU40
AY UU40

AX AC50000
AY AC50000
AX VL300
AY VL300

AA MR3,-3; GD
ID /XY

AA
AN0,0
CX

AX MR39; GD
ID /X
AY MR-4; GD
ID /Y

AX MR-39; GD
ID /X
AY MR-4; GD
ID /Y

AX MR39; GD
ID /X
AY MR-4; GD

ID /Y

AX MR-39; GD

ID /X

AY MR-4; GD

ID /Y

AX MR39; GD

ID /X

AY MR-4; GD

ID /Y

AX MR-39; GD

ID /X

AY MR-4; GD

ID /Y

AX MR39; GD

ID /X

AY MR-4; GD

ID /Y

AX MR-39; GD

ID /X

AY MR-4; GD

ID /Y

AX MR39; GD

ID /X

AY MR-4; GD

ID /Y

AX MR-39; GD

ID /X

AY MR-4; GD

ID /Y

AX MR39; GD

ID /X

AA

AF0,0

CX

AA MR3,-3; GD

ID /XY

AA

AN0,0

CX

AX MR-45; GD

ID /X

AY MR45; GD

ID /Y

AX MR45; GD

ID /X

AY MR-45; GD

ID /Y

AA

AF0,0

CX

*****move

AA MA150,-4290; GD

ID /Y

!XYZ

AY MR-4; GD
ID /Y

*****MOVE BOTTOM

CENTER

AX MR39; GD
ID /X

AX AC50000

AY MR-4; GD
ID /Y

AY AC50000

AX VL300

AY VL300

AX MR-39; GD
ID /X

*****50 UM PAD 50X 40*40

AY MR-4; GD
ID /Y

AA MR3,-3; GD

ID /XY

AX MR39; GD
ID /X

AA

AY MR-4; GD
ID /Y

AN0,0

CX

AX MR-39; GD
ID /X

AX MR39; GD

AY MR-4; GD
ID /Y

ID /X

AY MR-4; GD

ID /Y

AX MR39; GD
ID /X

AX MR-39; GD

AY MR-4; GD
ID /Y

ID /X

AY MR-4; GD

ID /Y

AX MR-39; GD
ID /X

AX MR39; GD

AY MR-4; GD
ID /Y

ID /X

AY MR-4; GD

ID /Y

AX MR39; GD
ID /X

AX MR-39; GD

ID /X

AA
AF0,0
CX

AY VL200

AA MR3,3; GD
ID /XY

*****50 UM PAD 50X 40*40

AX UF
AY UF

AA
AN0,0
CX

AX UU40
AY UU40

AX MR-45; GD
ID /X
AY MR45; GD
ID /Y
AX MR45; GD
ID /X
AY MR-45; GD
ID /Y

AX AC50000
AY AC50000
AX VL300
AY VL300

AA MR3,-3; GD
ID /XY

AA
AF0,0
CX

AA
AN0,0
CX

*****move
right

AX MR39; GD
ID /X
AY MR-4; GD
ID /Y

AA MA300,0; GD
ID /XY

AX MR-39; GD
ID /X
AY MR-4; GD
ID /Y

AX AC50000
AY AC50000
AX VL200

AX MR39; GD

ID /X
AY MR-4; GD
ID /Y

AX MR-39; GD
ID /X
AY MR-4; GD
ID /Y

AX MR39; GD
ID /X
AY MR-4; GD
ID /Y

AX MR-39; GD
ID /X
AY MR-4; GD
ID /Y

AX MR39; GD
ID /X
AY MR-4; GD
ID /Y

AX MR-39; GD
ID /X
AY MR-4; GD
ID /Y

AX MR39; GD
ID /X
AY MR-4; GD
ID /Y

AX MR-39; GD
ID /X

AY MR-4; GD
ID /Y

AX MR39; GD
ID /X

AA
AF0,0
CX

AA MR3,-3; GD
ID /XY

AA
AN0,0
CX

AX MR-45; GD
ID /X
AY MR45; GD
ID /Y
AX MR45; GD
ID /X
AY MR-45; GD
ID /Y

AA
AF0,0
CX

*****SIGNAL LINE
AX MR-13; GD
ID /X

AX AC50000

AY AC50000
AX VL200
AY VL200

AA
AN0,0
CX

AY MR-4250; GD
ID /Y

AX MR-5; GD
ID /X

AY MR4260; GD
ID /Y

AX MR-5; GD
ID /X

AY MR-4260; GD
ID /Y

AX MR-5; GD
ID /X

AY MR4260; GD
ID /Y

AA
AF0,0
CX

!XYZ

*****MOVE BOTTOM
CENTER

AA MA300,-4290; GD
ID /XY

!xyz

*****50 UMPAD 50X 40*40

AX AC50000
AY AC50000
AX VL300
AY VL300

AA
AN0,0
CX

AX MR39; GD
ID /X
AY MR-4; GD
ID /Y

AX MR-39; GD
ID /X
AY MR-4; GD
ID /Y

AX MR39; GD
ID /X
AY MR-4; GD
ID /Y

AX MR-39; GD
ID /X
AY MR-4; GD
ID /Y

AX MR39; GD
ID /X
AY MR-4; GD
ID /Y

AX MR-39; GD
ID /X
AY MR-4; GD
ID /Y

AX MR39; GD
ID /X
AY MR-4; GD
ID /Y

AX MR-39; GD
ID /X
AY MR-4; GD
ID /Y

AX MR39; GD
ID /X
AY MR-4; GD
ID /Y

AX MR-39; GD
ID /X
AY MR-4; GD
ID /Y

AX MR39; GD
ID /X

AA
AF0,0
CX

AA MR3,3; GD
ID /XY

AA
AN0,0
CX

AX MR-45; GD
ID /X
AY MR45; GD
ID /Y
AX MR45; GD
ID /X
AY MR-45; GD
ID /Y

AA
AF0,0
CX

AA MA170,-30; GD
ID /XY

*****set to 20X40

\$
*****SIGNAL LINE

AX AC50000
AY AC50000
AX VL200
AY VL200

AA
AN0,0
CX

AY MR-4265; GD
ID /Y

CX

!XYZ

AA
AF0,0

AA MA900,0; GD
ID /XY

File Name: MSG.txt

This file draws the ground lines for the MS

AX LP0
AY LP0

*****CALIBRATE

AX UF
AY UF

*Move in negative X direction

AX MR350 GO

ID

/X

AX UU40
AY UU40

~ad,25,32,16,4

#1 50000 0

AY MR-4500 GO

AX AC50000
AY AC50000

ID

/Y

AX VL600
AY VL600

~ad,25,32,16,4

#2 50000 50000

AX MR-350 GO

ID

/X	AX VL300
~ad,25,32,16,4	AY VL300
#3 0 50000	
AY MR4500 GO	
ID	
/Y	AA MR3,-3; GD
~ad,25,32,16,4	ID /XY
#4 0 0	
#5 0 0	AA
	AN0,0
*****LEFT GROUND	CX
AX LP0	
AY LP0	AX MR39; GD
	ID /X
AX UF	AY MR-4; GD
AY UF	ID /Y
AX UU40	AX MR-39; GD
AY UU40	ID /X
	AY MR-4; GD
AX AC50000	ID /Y
AY AC50000	
AX VL200	AX MR39; GD
AY VL200	ID /X
	AY MR-4; GD
	ID /Y
*****50 UM PAD 50X 40*40	AX MR-39; GD
AX UF	ID /X
AY UF	AY MR-4; GD
	ID /Y
AX UU40	
AY UU40	AX MR39; GD
	ID /X
AX AC50000	AY MR-4; GD
AY AC50000	ID /Y

AX MR-39; GD
ID /X
AY MR-4; GD
ID /Y

AX MR39; GD
ID /X
AY MR-4; GD
ID /Y

AX MR-39; GD
ID /X
AY MR-4; GD
ID /Y

AX MR39; GD
ID /X
AY MR-4; GD
ID /Y

AX MR-39; GD
ID /X
AY MR-4; GD
ID /Y

AX MR39; GD
ID /X

AA
AF0,0
CX

AA MR3,-3; GD
ID /XY

AA
AN0,0
CX

AX MR-45; GD
ID /X
AY MR45; GD
ID /Y
AX MR45; GD
ID /X
AY MR-45; GD
ID /Y

AA
AF0,0
CX

*****SIGNAL LINE

AA MR-21,3; GD
ID /XY

AX AC50000
AY AC50000
AX VL200
AY VL200

AA
AN0,0
CX

AY MR-4250; GD
ID /Y

AX MR-5; GD
ID /X

AY MR4255; GD
ID /Y

AA
AF0,0
CX

AY MR-4250; GD
ID /Y

!XYZ

*****MOVE BOTTOM
CENTER

AA MR-17,-3; GD
ID /XY
!xyz

*****50 UM PAD 50X 40*40

AX AC50000
AY AC50000
AX VL300
AY VL300

AA
AN0,0
CX

AX MR39; GD
ID /X
AY MR-4; GD
ID /Y

AX MR-39; GD
ID /X

AY MR-4; GD
ID /Y

AX MR39; GD
ID /X

AY MR-4; GD
ID /Y

AX MR-39; GD
ID /X
AY MR-4; GD
ID /Y

AX MR39; GD
ID /X
AY MR-4; GD
ID /Y

AX MR-39; GD
ID /X
AY MR-4; GD
ID /Y

AX MR39; GD
ID /X
AY MR-4; GD
ID /Y

AX MR-39; GD
ID /X
AY MR-4; GD
ID /Y

AX MR39; GD
ID /X
AY MR-4; GD
ID /Y

*****move
right

AX MR-39; GD
ID /X
AY MR-4; GD
ID /Y

AA MA300,0; GD
ID /XY

AX MR39; GD
ID /X

AX AC50000
AY AC50000
AX VL200
AY VL200

AA
AF0,0
CX

AA MR3,3; GD
ID /XY

*****50 UMPAD 50X 40*40
AX UF
AY UF

AA
AN0,0
CX

AX UU40
AY UU40

AX MR-45; GD
ID /X
AY MR45; GD
ID /Y
AX MR45; GD
ID /X
AY MR-45; GD
ID /Y

AX AC50000
AY AC50000
AX VL300
AY VL300

AA
AF0,0
CX

AA MR3,-3; GD
ID /XY

AA
AN0,0
CX

AX MR39; GD	AX MR-39; GD
ID /X	ID /X
AY MR-4; GD	AY MR-4; GD
ID /Y	ID /Y
AX MR-39; GD	AX MR39; GD
ID /X	ID /X
AY MR-4; GD	AY MR-4; GD
ID /Y	ID /Y
AX MR39; GD	AX MR-39; GD
ID /X	ID /X
AY MR-4; GD	AY MR-4; GD
ID /Y	ID /Y
AX MR-39; GD	AX MR39; GD
ID /X	ID /X
AY MR-4; GD	AY MR-4; GD
ID /Y	ID /Y
AX MR39; GD	AX MR39; GD
ID /X	ID /X
AY MR-4; GD	AY MR-4; GD
ID /Y	ID /Y
AX MR-39; GD	AX MR39; GD
ID /X	ID /X
AY MR-4; GD	AY MR-4; GD
ID /Y	ID /Y
AX MR39; GD	AA
ID /X	AF0,0
AY MR-4; GD	CX
ID /Y	AA MR3,-3; GD
AX MR-39; GD	ID /XY
ID /X	AA
AY MR-4; GD	AN0,0
ID /Y	CX
AX MR39; GD	AX MR-45; GD
ID /X	ID /X
AY MR-4; GD	AY MR45; GD
ID /Y	ID /Y
AX MR39; GD	AX MR45; GD
ID /X	ID /X

AY MR-45; GD

ID /Y

!XYZ

AA

AF0,0

CX

*****MOVE BOTTOM

CENTER

AA MR-17,-3; GD

ID /XY

!xyz

*****SIGNAL LINE

AA MR-21,3; GD

ID /XY

*****50 UM PAD 50X 40*40

AX AC50000

AY AC50000

AX VL200

AY VL200

AX AC50000

AY AC50000

AX VL300

AY VL300

AA

AN0,0

CX

AA

AN0,0

CX

AY MR-4250; GD

ID /Y

AX MR39; GD

ID /X

AX MR-5; GD

ID /X

AY MR-4; GD

ID /Y

AY MR4255; GD

ID /Y

AX MR-39; GD

ID /X

AA

AF0,0

CX

AY MR-4; GD

ID /Y

AY MR-4250; GD

ID /Y

AX MR39; GD

ID /X

AY MR-4; GD

ID /Y

AX MR-39; GD
ID /X
AY MR-4; GD
ID /Y

AX MR39; GD
ID /X
AY MR-4; GD
ID /Y

AX MR-39; GD
ID /X
AY MR-4; GD
ID /Y

AX MR39; GD
ID /X
AY MR-4; GD
ID /Y

AX MR-39; GD
ID /X
AY MR-4; GD
ID /Y

AX MR39; GD
ID /X
AY MR-4; GD
ID /Y

AX MR-39; GD
ID /X

AY MR-4; GD
ID /Y

AX MR39; GD
ID /X

AA
AF0,0
CX

AA MR3,3; GD
ID /XY

AA
AN0,0
CX

AX MR-45; GD
ID /X
AY MR45; GD
ID /Y
AX MR45; GD
ID /X
AY MR-45; GD
ID /Y

AA
AF0,0
CX

AA MA900,0; GD
ID /XY

File Name: mst.txt

This file draws a 200 micron thru line

```
AX LP0 /X
AY LP0 ~ad,25,32,16,4
#3 0 50000
AX UF AY MR200 GO
AY UF ID
/Y
AX UU40 ~ad,25,32,16,4
AY UU40 #4 0 0
#5 0 0
AX AC50000
AY AC50000 *****LEFT GROUND
AX VL600 AX LP0
AY VL600 AY LP0
AX UF
*****CALIBRATE AY UF
*Move in negative X direction AX UU40
AX MR350 GO AY UU40
ID
/X AX AC50000
~ad,25,32,16,4 AY AC50000
#1 50000 0 AX VL200
AY MR-200 GO AY VL200
ID
/Y
~ad,25,32,16,4
#2 50000 50000 *****50 UM PAD 50X 40*40
AX MR-350 GO AX UF
ID AY UF
```

AX UU40

AY UU40

AX AC50000

AY AC50000

AX VL300

AY VL300

AA MR3,-3; GD

ID /XY

AA

AN0,0

CX

AX MR39; GD

ID /X

AY MR-4; GD

ID /Y

AX MR-39; GD

ID /X

AY MR-4; GD

ID /Y

AX MR39; GD

ID /X

AY MR-4; GD

ID /Y

AX MR-39; GD

ID /X

AY MR-4; GD

ID /Y

AX MR39; GD

ID /X

AY MR-4; GD

ID /Y

AX MR-39; GD

ID /X

AY MR-4; GD

ID /Y

AX MR39; GD

ID /X

AY MR-4; GD

ID /Y

AX MR-39; GD

ID /X

AY MR-4; GD

ID /Y

AX MR39; GD

ID /X

AY MR-4; GD

ID /Y

AX MR-39; GD

ID /X

AY MR-4; GD

ID /Y

AX MR39; GD

ID /X

AA

AF0,0
CX

AA MR3,-3; GD
ID /XY

AA
AN0,0
CX

AX MR-45; GD
ID /X
AY MR45; GD
ID /Y
AX MR45; GD
ID /X
AY MR-45; GD
ID /Y

AA
AF0,0
CX

AA MR-3,3; GD
ID /XY

*****SIGNAL LINE

AX MR-13; GD
ID /X

AX AC50000
AY AC50000
AX VL200
AY VL200

AA
AN0,0
CX

AY MR-150; GD
ID /Y

AX MR-5; GD
ID /X

AY MR155; GD
ID /Y

AX MR-5; GD
ID /X

AY MR-150; GD
ID /Y

AX MR-5; GD
ID /X

AY MR150; GD
ID /Y

AA
AF0,0
CX

AY MR-150; GD
ID /Y

!XYZ

*****MOVE BOTTOM
CENTER

AA MR-12,-3; GD

ID /XY

!xyz

*****50 UMPAD 50X 40*40

AX AC50000

AY AC50000

AX VL300

AY VL300

AA

AN0,0

CX

AX MR39; GD

ID /X

AY MR-4; GD

ID /Y

AX MR-39; GD

ID /X

AY MR-4; GD

ID /Y

AX MR39; GD

ID /X

AY MR-4; GD

ID /Y

AX MR-39; GD

ID /X

AY MR-4; GD

ID /Y

AX MR39; GD

ID /X

AY MR-4; GD

ID /Y

AX MR-39; GD

ID /X

AY MR-4; GD

ID /Y

AX MR39; GD

ID /X

AY MR-4; GD

ID /Y

AX MR-39; GD

ID /X

AY MR-4; GD

ID /Y

AX MR39; GD

ID /X

AY MR-4; GD

ID /Y

AX MR-39; GD

ID /X

AY MR-4; GD

ID /Y

AX MR39; GD

ID /X

AA

AF0,0

CX

AY UF

AA MR3,3; GD
ID /XY

AX UU40
AY UU40

AA
AN0,0
CX

AX AC50000
AY AC50000
AX VL300
AY VL300

AX MR-45; GD
ID /X
AY MR45; GD
ID /Y
AX MR45; GD
ID /X
AY MR-45; GD
ID /Y

AA MR3,-3; GD
ID /XY

AA
AN0,0
CX

AA
AF0,0
CX

AX MR39; GD
ID /X
AY MR-4; GD
ID /Y

*****sig pads

AX AC50000
AY AC50000
AX VL200
AY VL200

AX MR-39; GD
ID /X
AY MR-4; GD
ID /Y

*****move

AA MA150,0; GD
ID /XY

AX MR39; GD
ID /X
AY MR-4; GD
ID /Y

*****50 UM PAD 50X 40*40

AX UF

AX MR-39; GD
ID /X
AY MR-4; GD

ID /Y

AX MR39; GD

ID /X

AY MR-4; GD

ID /Y

AX MR-39; GD

ID /X

AY MR-4; GD

ID /Y

AX MR39; GD

ID /X

AY MR-4; GD

ID /Y

AX MR-39; GD

ID /X

AY MR-4; GD

ID /Y

AX MR39; GD

ID /X

AY MR-4; GD

ID /Y

AX MR-39; GD

ID /X

AY MR-4; GD

ID /Y

AX MR39; GD

ID /X

AA

AF0,0

CX

AA MR3,-3; GD

ID /XY

AA

AN0,0

CX

AX MR-45; GD

ID /X

AY MR45; GD

ID /Y

AX MR45; GD

ID /X

AY MR-45; GD

ID /Y

AA

AF0,0

CX

*****MOVE BOTTOM
CENTER

AA MA150,-190; GD

ID /XY

!xyz

*****50 UM PAD 50X 40*40

AX AC50000

AY AC50000

AX VL300

AY VL300

AA MR3,-3; GD ID /XY	AY MR-4; GD ID /Y
AA AN0,0 CX	AX MR39; GD ID /X AY MR-4; GD ID /Y
AX MR39; GD ID /X AY MR-4; GD ID /Y	AX MR-39; GD ID /X AY MR-4; GD ID /Y
AX MR-39; GD ID /X AY MR-4; GD ID /Y	AX MR39; GD ID /X AY MR-4; GD ID /Y
AX MR39; GD ID /X AY MR-4; GD ID /Y	AX MR-39; GD ID /X AY MR-4; GD ID /Y
AX MR-39; GD ID /X AY MR-4; GD ID /Y	AX MR39; GD ID /X AY MR-4; GD ID /Y
AX MR39; GD ID /X AY MR-4; GD ID /Y	AX MR-39; GD ID /X AY MR-4; GD ID /Y
AX MR-39; GD ID /X AY MR-4; GD ID /Y	AA AF0,0 CX
AX MR39; GD ID /X AY MR-4; GD ID /Y	AA MR3,3; GD ID /XY
AX MR-39; GD ID /X	AA AN0,0 CX

AX MR-45; GD
ID /X
AY MR45; GD
ID /Y
AX MR45; GD
ID /X
AY MR-45; GD
ID /Y

AA
AF0,0
CX

*****move
right

AA MA300,0; GD
ID /XY

AX AC50000
AY AC50000
AX VL200
AY VL200

*****50 UM PAD 50X 40*40

AX UF
AY UF

AX UU40
AY UU40

AX AC50000
AY AC50000
AX VL300
AY VL300

AA MR3,-3; GD
ID /XY

AA
AN0,0
CX

AX MR39; GD
ID /X
AY MR-4; GD
ID /Y

AX MR-39; GD
ID /X
AY MR-4; GD
ID /Y

AX MR39; GD
ID /X
AY MR-4; GD
ID /Y

AX MR-39; GD
ID /X
AY MR-4; GD
ID /Y

AX MR39; GD
ID /X
AY MR-4; GD

ID /Y

ID /XY

AX MR-39; GD

AA

ID /X

AN0,0

AY MR-4; GD

CX

ID /Y

AX MR-45; GD

AX MR39; GD

ID /X

ID /X

AY MR45; GD

AY MR-4; GD

ID /Y

ID /Y

AX MR45; GD

AX MR-39; GD

ID /X

ID /X

AY MR-45; GD

AY MR-4; GD

ID /Y

ID /Y

AA

AX MR39; GD

AF0,0

ID /X

CX

AY MR-4; GD

AA MR-3,3; GD

ID /Y

ID /XY

AX MR-39; GD

*****SIGNAL LINE

ID /X

AX MR-13; GD

AY MR-4; GD

ID /X

ID /Y

AX MR39; GD

AX AC50000

ID /X

AY AC50000

AX VL200

AY VL200

AA

AA

AF0,0

AN0,0

CX

CX

AA MR3,-3; GD

AY MR-150; GD
ID /Y

AX MR-5; GD
ID /X

AY MR155; GD
ID /Y

AX MR-5; GD
ID /X

AY MR-150; GD
ID /Y

AX MR-5; GD
ID /X

AY MR150; GD
ID /Y

AA
AF0,0
CX

AY MR-150; GD
ID /Y

!XYZ

*****MOVE BOTTOM
CENTER

AA MR-12,-3; GD
ID /XY

!xyz

*****50 UM PAD 50X 40*40

AX AC50000

AY AC50000

AX VL300

AY VL300

AA

AN0,0

CX

AX MR39; GD

ID /X

AY MR-4; GD

ID /Y

AX MR-39; GD

ID /X

AY MR-4; GD

ID /Y

AX MR39; GD

ID /X

AY MR-4; GD

ID /Y

AX MR-39; GD

ID /X

AY MR-4; GD

ID /Y

AX MR39; GD

ID /X

AY MR-4; GD

ID /Y

AX MR-39; GD

ID /X

AY MR-4; GD

ID /Y

AX MR39; GD

ID /X

AY MR-4; GD

ID /Y

AX MR-39; GD

ID /X

AY MR-4; GD

ID /Y

AX MR39; GD

ID /X

AY MR-4; GD

ID /Y

AX MR-39; GD

ID /X

AY MR-4; GD

ID /Y

AX MR39; GD

ID /X

AA

AF0,0

CX

AA MR3,3; GD

ID /XY

AA

AN0,0

CX

AX MR-45; GD

ID /X

AY MR45; GD

ID /Y

AX MR45; GD

ID /X

AY MR-45; GD

ID /Y

AA

AF0,0

CX

AA MA170,-30; GD

ID /XY

*****set to 20X40

\$

AX AC50000

AY AC50000

AX VL200

AY VL200

AA

AN0,0

CX

AY MR-165; GD

ID /Y

AA	I XYZ
AF0,0	AA MA900,0; GD
CX	ID /XY

File Name: mstg.txt

This file draws the ground lines for the thru line

AX LP0	AY MR-4500 GO
AY LP0	ID
	/Y
	~ad,25,32,16,4
AX UF	#2 50000 50000
AY UF	AX MR-350 GO
	ID
AX UU40	/X
AY UU40	~ad,25,32,16,4
	#3 0 50000
AX AC50000	AY MR4500 GO
AY AC50000	ID
AX VL600	/Y
AY VL600	~ad,25,32,16,4
	#4 0 0
	#5 0 0
*****CALIBRATE	*****LEFT GROUND
*Move in negative X direction	AX LP0
AX MR350 GO	AY LP0
ID	
/X	AX UF
~ad,25,32,16,4	AY UF
#1 50000 0	

AX UU40	ID /X
AY UU40	AY MR-4; GD
	ID /Y
AX AC50000	
AY AC50000	AX MR39; GD
AX VL200	ID /X
AY VL200	AY MR-4; GD
	ID /Y
	AX MR-39; GD
*****50 UM PAD 50X 40*40	ID /X
AX UF	AY MR-4; GD
AY UF	ID /Y
AX UU40	AX MR39; GD
AY UU40	ID /X
	AY MR-4; GD
AX AC50000	ID /Y
AY AC50000	
AX VL300	AX MR-39; GD
AY VL300	ID /X
	AY MR-4; GD
	ID /Y
AA MR3,-3; GD	
ID /XY	AX MR39; GD
AA	ID /X
AN0,0	AY MR-4; GD
CX	ID /Y
	AX MR-39; GD
AX MR39; GD	ID /X
ID /X	AY MR-4; GD
AY MR-4; GD	ID /Y
ID /Y	
AX MR-39; GD	AX MR39; GD
	ID /X

AY MR-4; GD
ID /Y

AX MR-39; GD
ID /X
AY MR-4; GD
ID /Y

AX MR39; GD
ID /X

AA
AF0,0
CX

AA MR3,-3; GD
ID /XY

AA
AN0,0
CX

AX MR-45; GD
ID /X
AY MR45; GD
ID /Y
AX MR45; GD
ID /X
AY MR-45; GD
ID /Y

AA
AF0,0
CX

AA MR-3,3; GD
ID /XY

*****SIGNAL LINE
AX MR-18; GD
ID /X

AX AC50000
AY AC50000
AX VL200
AY VL200

AA
AN0,0
CX

AY MR-150; GD
ID /Y

AX MR-5; GD
ID /X

AY MR155; GD
ID /Y

AA
AF0,0
CX

AY MR-150; GD
ID /Y

!XYZ

*****MOVE BOTTOM
CENTER

AA MR-17,-3; GD

ID /XY

!xyz

*****50 UM PAD 50X 40*40

AX AC50000

AY AC50000

AX VL300

AY VL300

AA

AN0,0

CX

AX MR39; GD

ID /X

AY MR-4; GD

ID /Y

AX MR-39; GD

ID /X

AY MR-4; GD

ID /Y

AX MR39; GD

ID /X

AY MR-4; GD

ID /Y

AX MR-39; GD

ID /X

AY MR-4; GD

ID /Y

AX MR39; GD

ID /X

AY MR-4; GD

ID /Y

AX MR-39; GD

ID /X

AY MR-4; GD

ID /Y

AX MR39; GD

ID /X

AY MR-4; GD

ID /Y

AX MR-39; GD

ID /X

AY MR-4; GD

ID /Y

AX MR39; GD

ID /X

AY MR-4; GD

ID /Y

AX MR-39; GD

ID /X

AY MR-4; GD

ID /Y

AX MR39; GD

ID /X

AA

AF0,0	
CX	*****50 UM PAD 50X 40*40
	AX UF
AA MR3,3; GD	AY UF
ID /XY	
	AX UU40
AA	AY UU40
AN0,0	
CX	AX AC50000
	AY AC50000
AX MR-45; GD	AX VL300
ID /X	AY VL300
AY MR45; GD	
ID /Y	
AX MR45; GD	AA MR3,-3; GD
ID /X	ID /XY
AY MR-45; GD	
ID /Y	AA
	AN0,0
AA	CX
AF0,0	
CX	AX MR39; GD
	ID /X
	AY MR-4; GD
	ID /Y
*****move	
right	
	AX MR-39; GD
AA MA300,0; GD	ID /X
ID /XY	AY MR-4; GD
	ID /Y
AX AC50000	AX MR39; GD
AY AC50000	ID /X
AX VL200	AY MR-4; GD
AY VL200	ID /Y

AX MR-39; GD
ID /X
AY MR-4; GD
ID /Y

ID /X

AA
AF0,0
CX

AX MR39; GD
ID /X
AY MR-4; GD
ID /Y

AA MR3,-3; GD
ID /XY

AX MR-39; GD
ID /X
AY MR-4; GD
ID /Y

AA
AN0,0
CX

AX MR39; GD
ID /X
AY MR-4; GD
ID /Y

AX MR-45; GD
ID /X
AY MR45; GD
ID /Y
AX MR45; GD
ID /X

AX MR-39; GD
ID /X
AY MR-4; GD
ID /Y

AY MR-45; GD
ID /Y

AX MR39; GD
ID /X
AY MR-4; GD
ID /Y

AA
AF0,0
CX

AX MR-39; GD
ID /X
AY MR-4; GD
ID /Y

AA MR-3,3; GD
ID /XY

AX MR39; GD

*****SIGNAL LINE
AX MR-18; GD
ID /X

AX AC5000

AY AC50000
AX VL200
AY VL200

AX VL300
AY VL300

AA
AN0,0
CX

AA
AN0,0
CX

AY MR-150; GD
ID /Y

AX MR39; GD
ID /X

AX MR-5; GD
ID /X

AY MR-4; GD
ID /Y

AY MR155; GD
ID /Y

AX MR-39; GD
ID /X
AY MR-4; GD
ID /Y

AA
AF0,0
CX

AX MR39; GD
ID /X

AY MR-150; GD
ID /Y

AY MR-4; GD
ID /Y

!XYZ

AX MR-39; GD
ID /X

*****MOVE BOTTOM
CENTER

AY MR-4; GD
ID /Y

AA MR-17,-3; GD
ID /XY
!xyz

AX MR39; GD
ID /X
AY MR-4; GD
ID /Y

*****50 UM PAD 50X 40*40

AX MR-39; GD
ID /X

AX AC50000
AY AC50000

AY MR-4; GD
ID /Y

AX MR39; GD
ID /X
AY MR-4; GD
ID /Y

AX MR-39; GD
ID /X
AY MR-4; GD
ID /Y

AX MR39; GD
ID /X
AY MR-4; GD
ID /Y

AX MR-39; GD
ID /X
AY MR-4; GD
ID /Y

AX MR39; GD
ID /X

AA
AF0,0
CX

AA MR3,3; GD
ID /XY

AA
AN0,0
CX

AX MR-45; GD
ID /X
AY MR45; GD
ID /Y
AX MR45; GD
ID /X
AY MR-45; GD
ID /Y

AA
AF0,0
CX

AA MA900,0; GD
ID /XY

File Name: MSR.txt

This file draws a reflect line and used msg.txt for the ground lines

AX LP0	~ad,25,32,16,4
AY LP0	#4 0 0
	#5 0 0
AX UF	
AY UF	*****LEFT GROUND
	AX LP0
	AY LP0
AX UU40	
AY UU40	
	AX UF
	AY UF
AX AC50000	
AY AC50000	
AX VL600	AX UU40
AY VL600	AY UU40
	AX AC50000
*****CALIBRATE	AY AC50000
	AX VL200
	AY VL200
*Move in negative X direction	
AX MR350 GO	
ID	
/X	
~ad,25,32,16,4	*****50 UM PAD 50X 40*40
#1 50000 0	AX UF
AY MR-4290 GO	AY UF
ID	
/Y	AX UU40
~ad,25,32,16,4	AY UU40
#2 50000 50000	
AX MR-350 GO	AX AC50000
ID	AY AC50000
/X	AX VL300
~ad,25,32,16,4	AY VL300
#3 0 50000	
AY MR4290 GO	
ID	
/Y	AA MR3,-3; GD

ID /XY

AA

AN0,0

CX

AX MR39; GD

ID /X

AY MR-4; GD

ID /Y

AX MR-39; GD

ID /X

AY MR-4; GD

ID /Y

AX MR39; GD

ID /X

AY MR-4; GD

ID /Y

AX MR-39; GD

ID /X

AY MR-4; GD

ID /Y

AX MR39; GD

ID /X

AY MR-4; GD

ID /Y

AX MR-39; GD

ID /X

AY MR-4; GD

ID /Y

AX MR39; GD

ID /X

AY MR-4; GD

ID /Y

AX MR-39; GD

ID /X

AY MR-4; GD

ID /Y

AX MR39; GD

ID /X

AY MR-4; GD

ID /Y

AX MR-39; GD

ID /X

AY MR-4; GD

ID /Y

AX MR39; GD

ID /X

AA

AF0,0

CX

AA MR3,-3; GD

ID /XY

AA

AN0,0

CX

AX MR-45; GD

ID /X
AY MR45; GD
ID /Y
AX MR45; GD
ID /X
AY MR-45; GD
ID /Y

AA
AF0,0
CX

*****SIGNAL LINE

AX MR-13; GD
ID /X

AX AC50000
AY AC50000
AX VL200
AY VL200

AA
AN0,0
CX

AY MR-4250; GD
ID /Y

AX MR-5; GD
ID /X

AY MR4260; GD
ID /Y

AX MR-5; GD
ID /X

AY MR-4260; GD
ID /Y

AX MR-5; GD
ID /X

AY MR4260; GD
ID /Y

AA
AF0,0
CX

!XYZ

*****MOVE BOTTOM
CENTER

AA MA0,-4290; GD
ID /XY

!xyz

*****50 UM PAD 50X 40*40

AX AC50000
AY AC50000
AX VL300
AY VL300

AA
AN0,0
CX

AX MR39; GD
ID /X

AY MR-4; GD
ID /Y

AX MR-39; GD
ID /X
AY MR-4; GD
ID /Y

AX MR39; GD
ID /X
AY MR-4; GD
ID /Y

AX MR-39; GD
ID /X
AY MR-4; GD
ID /Y

AX MR39; GD
ID /X
AY MR-4; GD
ID /Y

AX MR-39; GD
ID /X
AY MR-4; GD
ID /Y

AX MR39; GD
ID /X
AY MR-4; GD
ID /Y

AX MR-39; GD
ID /X
AY MR-4; GD

ID /Y

AX MR39; GD
ID /X
AY MR-4; GD
ID /Y

AX MR-39; GD
ID /X
AY MR-4; GD
ID /Y

AX MR39; GD
ID /X

AA
AF0,0
CX

AA MR3,3; GD
ID /XY

AA
AN0,0
CX

AX MR-45; GD
ID /X
AY MR45; GD
ID /Y
AX MR45; GD
ID /X
AY MR-45; GD
ID /Y

AA

AF0,0	
CX	AX MR39; GD
*****sig pads	ID /X
AA MA150,0; GD	AY MR-4; GD
ID /XY	ID /Y
*****50 UM PAD 50X 40*40	AX MR-39; GD
AX UF	ID /X
AY UF	AY MR-4; GD
	ID /Y
AX UU40	
AY UU40	AX MR39; GD
	ID /X
AX AC50000	AY MR-4; GD
AY AC50000	ID /Y
AX VL300	
AY VL300	AX MR-39; GD
	ID /X
	AY MR-4; GD
	ID /Y
AA MR3,-3; GD	
ID /XY	AX MR39; GD
	ID /X
AA	AY MR-4; GD
AN0,0	ID /Y
CX	
	AX MR-39; GD
AX MR39; GD	ID /X
ID /X	AY MR-4; GD
AY MR-4; GD	ID /Y
ID /Y	
	AX MR39; GD
AX MR-39; GD	ID /X
ID /X	AY MR-4; GD
AY MR-4; GD	ID /Y
ID /Y	

AX MR-39; GD
ID /X
AY MR-4; GD
ID /Y

AX MR39; GD
ID /X

AA
AF0,0
CX

AA MR3,-3; GD
ID /XY

AA
AN0,0
CX

AX MR-45; GD
ID /X
AY MR45; GD
ID /Y
AX MR45; GD
ID /X
AY MR-45; GD
ID /Y

AA
AF0,0
CX

*****move

AA MA150,-4290; GD
ID /Y

!XYZ

*****MOVE BOTTOM
CENTER

AX AC50000
AY AC50000
AX VL300
AY VL300

*****50 UM PAD 50X 40*40

AA MR3,-3; GD
ID /XY

AA
AN0,0
CX

AX MR39; GD
ID /X
AY MR-4; GD
ID /Y

AX MR-39; GD
ID /X
AY MR-4; GD
ID /Y

AX MR39; GD
ID /X
AY MR-4; GD

ID /Y

AX MR-39; GD

ID /X

AY MR-4; GD

ID /Y

AX MR39; GD

ID /X

AY MR-4; GD

ID /Y

AX MR-39; GD

ID /X

AY MR-4; GD

ID /Y

AX MR39; GD

ID /X

AY MR-4; GD

ID /Y

AX MR-39; GD

ID /X

AY MR-4; GD

ID /Y

AX MR39; GD

ID /X

AY MR-4; GD

ID /Y

AX MR-39; GD

ID /X

AY MR-4; GD

ID /Y

AX MR39; GD

ID /X

AA

AF0,0

CX

AA MR3,3; GD

ID /XY

AA

AN0,0

CX

AX MR-45; GD

ID /X

AY MR45; GD

ID /Y

AX MR45; GD

ID /X

AY MR-45; GD

ID /Y

AA

AF0,0

CX

*****move
right

AA MA300,0; GD

ID /XY

AX AC50000	AY MR-4; GD
AY AC50000	ID /Y
AX VL200	AX MR39; GD
AY VL200	ID /X
	AY MR-4; GD
	ID /Y
*****50 UMPAD 50X 40*40	
AX UF	AX MR-39; GD
AY UF	ID /X
	AY MR-4; GD
	ID /Y
AX UU40	
AY UU40	AX MR39; GD
	ID /X
AX AC50000	AY MR-4; GD
AY AC50000	ID /Y
AX VL300	
AY VL300	AX MR-39; GD
	ID /X
	AY MR-4; GD
	ID /Y
AA MR3,-3; GD	
ID /XY	AX MR39; GD
	ID /X
AA	AY MR-4; GD
AN0,0	ID /Y
CX	
	AX MR-39; GD
AX MR39; GD	ID /X
ID /X	AY MR-4; GD
AY MR-4; GD	ID /Y
ID /Y	
	AX MR39; GD
AX MR-39; GD	ID /X
ID /X	AY MR-4; GD

ID /Y

AX MR-39; GD

ID /X

AY MR-4; GD

ID /Y

AX MR39; GD

ID /X

AA

AF0,0

CX

AA MR3,-3; GD

ID /XY

AA

AN0,0

CX

AX MR-45; GD

ID /X

AY MR45; GD

ID /Y

AX MR45; GD

ID /X

AY MR-45; GD

ID /Y

AA

AF0,0

CX

*****SIGNAL LINE

AX MR-13; GD

ID /X

AX AC50000

AY AC50000

AX VL200

AY VL200

AA

AN0,0

CX

AY MR-4250; GD

ID /Y

AX MR-5; GD

ID /X

AY MR4260; GD

ID /Y

AX MR-5; GD

ID /X

AY MR-4260; GD

ID /Y

AX MR-5; GD

ID /X

AY MR4260; GD

ID /Y

AA

AF0,0

CX

	AX MR-39; GD
	ID /X
!XYZ	AY MR-4; GD
	ID /Y
*****MOVE BOTTOM	
CENTER	AX MR39; GD
AA MA300,-4290; GD	ID /X
ID /XY	AY MR-4; GD
!xyz	ID /Y

*****50 UM PAD 50X 40*40	AX MR-39; GD
AX AC50000	ID /X
AY AC50000	AY MR-4; GD
AX VL300	ID /Y
AY VL300	
	AX MR39; GD
	ID /X
AA	AY MR-4; GD
AN0,0	ID /Y
CX	
	AX MR-39; GD
	ID /X
AX MR39; GD	AY MR-4; GD
ID /X	ID /Y
AY MR-4; GD	
ID /Y	AX MR39; GD
	ID /X
AX MR-39; GD	AY MR-4; GD
ID /X	ID /Y
AY MR-4; GD	
ID /Y	AX MR-39; GD
	ID /X
AX MR39; GD	AY MR-4; GD
ID /X	ID /Y
AY MR-4; GD	
ID /Y	AX MR39; GD

ID /X	AX VL200
	AY VL200
AA	
AF0,0	AA
CX	AN0,0
	CX
AA MR3,3; GD	
ID /XY	AY MR-315; GD
	ID /Y
AA	
AN0,0	AA
CX	AF0,0
	CX
AX MR-45; GD	
ID /X	AY MR-3645; GD
AY MR45; GD	ID /Y
ID /Y	
AX MR45; GD	AA
ID /X	AN0,0
AY MR-45; GD	CX
ID /Y	
	AY MR-315; GD
AA	ID /Y
AF0,0	
CX	AA
	AF0,0
AA MA170,-30; GD	CX
ID /XY	
*****set to 20X40	!XYZ
\$	
*****SIGNAL LINE	AA MA900,0; GD
AX AC50000	ID /XY
AY AC50000	

File Name: Short.txt

This file draws a pair of shorts.

ID /XY	ID
	/X
AX LP0	~ad,25,32,16,4
AY LP0	#1 50000 0
	AY MR-270 GO
AX UF	ID
AY UF	/Y
	~ad,25,32,16,4
AX UU40	#2 50000 50000
AY UU40	AX MR-650 GO
	ID
AX AC50000	/X
AY AC50000	~ad,25,32,16,4
AX VL200	#3 0 50000
AY VL200	AY MR270 GO
	ID
	/Y
*****CALIBRATE	~ad,25,32,16,4
AX UF	#4 0 0
AY UF	#5 0 0
AX UU40	*****
AY UU40	AX LP0
	AY LP0
*Move in negative X direction	
AY AC500	AX UF
AX AC500	AY UF
AX VL250	
AY VL250	AX UU40
AX MR650 GO	AY UU40

AX AC50000	ID /X
AY AC50000	AY MR-4; GD
AX VL200	ID /Y
AY VL200	AX MR-650; GD
	ID /X
	AY MR-4; GD
	ID /Y
AA	AX MR650; GD
AN0,0	ID /X
CX	AY MR-4; GD
	ID /Y
AX MR650; GD	AX MR-650; GD
ID /X	ID /X
AY MR-4; GD	AY MR-2; GD
ID /Y	ID /Y
AX MR-650; GD	AX MR650; GD
ID /X	ID /X
AY MR-4; GD	
ID /Y	AA
AX MR650; GD	AF0,0
ID /X	CX
AY MR-4; GD	
ID /Y	!XYZ
AX MR-650; GD	
ID /X	AA MT0,-320; GD
AY MR-4; GD	ID /XY
ID /Y	
AX MR650; GD	AA
ID /X	AN0,0
AY MR-4; GD	CX
ID /Y	
AX MR-650; GD	AX MR650; GD
ID /X	ID /X
AY MR-4; GD	AY MR-4; GD
ID /Y	ID /Y
AX MR650; GD	AX MR-650; GD

ID /X
AY MR-4; GD
ID /Y
AX MR650; GD
ID /X
AY MR-4; GD
ID /Y
AX MR-650; GD
ID /X
AY MR-4; GD
ID /Y
AX MR650; GD
ID /X
AY MR-4; GD
ID /Y
AX MR-650; GD
ID /X
AY MR-4; GD
ID /Y
AX MR650; GD
ID /X
AY MR-4; GD
ID /Y
AX MR-650; GD
ID /X
AY MR-2; GD
ID /Y
AX MR650; GD

ID /X

AA
AF0,0
CX

AA MT900,0; GD
ID /XY

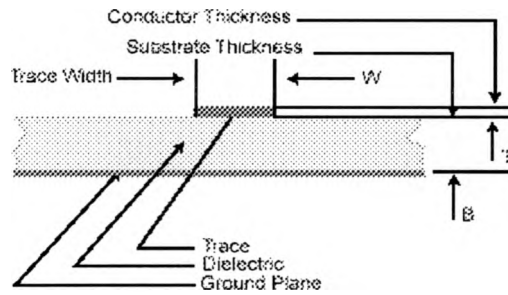
APPENDIX D

MICROSTRIP ϵ_{eff} CALCULATION

[<http://www.rogers-corp.com/mwu/pdf/tm333.pdf>]

Unlike the stripline configuration where the strip lies between two ground planes, transmission lines in microstrip are not entirely in the TEM mode and tend to be dispersive. That is, the effective dielectric constant and the impedance vary with the frequency of the transmitted signal. The effect is especially pronounced when the frequency is near the TEM cutoff frequency. Several papers have been written dealing with the microstrip transmission line. The static electric field computer analysis of Bryant and Weiss (1,2) is accepted as highly accurate, but lacking in frequency effect and time-consuming in computation. The standard closed form solutions of Wheeler (3) and Schneider (4) have been improved in accuracy by Hammerstad (5) and a summary of accurate closed form equations, including the effect of frequency, have been presented by Hammerstad and Jensen (6). Improved formulas for the frequency dispersion effect were published by Kirschning and Jansen (7). These were experimentally evaluated by Debele and Bayer (8), who reported better prediction of results, especially at higher frequencies. The formulas in (6) with dispersion according to (7) were used in this revision. References 1, 6 are included in the collection of reference 9.

1. T.G. Bryant and J.A. Weiss, "Parameters of Microstrip Transmission Lines and Coupled Pairs of Microstrip Lines". IEEE Trans MTT, MTT-16 (Dec. 1988) pp 1021-27.
2. T.G. Bryant and J.A. Weiss, "MSTRIP (Parameters of Microstrip)", IEEE Trans MTT, Computer Prog Desc. (Apr. 1971) pp 418-419.
3. H.A. Wheeler, "Transmission Line Properties of Parallel Strips Separated by a Dielectric Sheet", IEEE Trans MTT, (Mar. 1965) pp 172-185.
4. M.V. Schneider, "Microstrip Lines for Microwave Integrated Circuits", The Bell System Technical Journal, (May-June 1969) PP 1421-44.
5. E.O. Hammerstad, "Equations for Microstrip Circuit Design", Proceedings of 5th European Microwave Conference, (Sept 1-4, 1975) Hamburg, Germany, pp 268-72.
6. E. Hammerstad and O. Jensen, "Accurate Models for Microstrip Computer-Aided Design", 1980 IEEE MTT-S International Symposium Digest, (May 1980) Washington D.C. IEEE catalog #80CH1545-3MTT, pp 407-409.
7. M. Kirschning and R.H. Jansen, Electronics Letters, (18 March 1982) Vol 18, No. 6, pp 272-273.
8. S. Debele, J.B. Bayer, IEEE Trans MTT, Vol MTT-35, No. 5, (May 1987) pp 535-538.
9. PLANAR TRANSMISSION LINE STRUCTURES, Ed, T. Itoh, 1987 IEEE Pres.



- B = substrate thickness in millimeters
- T = ratio of conductor thickness to substrate thickness
- W = ratio of trace width to substrate thickness
- F = frequency in GHz
- εr = relative permittivity
- εeff0 = effective relative permittivity at 0 frequency
- εeffF = effective relative permittivity at frequency F
- Z0 = characteristic impedance at 0 frequency
- Zc,F = characteristic impedance at frequency F
- η0 = 376.73
- P = filling factor
- c = speed of light : 299 792 mm/ns
- e = natural logarithm base

Get width corrected for thickness in homogeneous medium:

$$U_1 = U_0 + \frac{7 \ln(1 + \frac{4c}{T} \tanh^2((6.517T)^{0.5}))}{\pi}$$

Get width corrected for mixed media

$$U_2 = U_1 + \frac{(U_1 - U_0)(1 + \frac{1}{\cosh((\epsilon_r - 1)^{0.5}))})}{2}$$

Use U₂ and ε_r to get value for intermediate Y

$$Y = \frac{\epsilon_r + 1}{2} + \frac{\epsilon_r - 1}{2} \left(1 + \frac{10}{U_2} \right)^{-0.4869 U_2}$$

Get Z₀ without frequency effect

$$Z_0 = 1 + \frac{\ln\left(\frac{U_2^2 + \frac{U_2^2}{2704}}{U_2^2 + 0.432}\right) + \ln\left(\frac{U_2}{18.1}\right) + 1}{49} + \frac{1}{18.7}$$

$$B_{eff} = 0.564 \left(\frac{\epsilon_r - 1.0}{\epsilon_r + 3} \right)^{0.811}$$

$$Z_{0f} = \frac{Z_0(U_{2f})}{Y^{0.5}}$$

Where Z_{0f} (arg) is given by

$$Z_{0f}(F) = \frac{\eta_0 \ln\left[\frac{(b + (2\pi \cdot 6 \times \frac{30,000}{F})^{0.5}))}{a} + \left(\frac{a}{a^2} + 1\right)^{0.5} \right]}{2\pi}$$

Get effective permittivity without frequency effect

$$\epsilon_{eff0} = Y \left(\frac{Z_0(U_{2f})}{Z_{0f}(F)} \right)^2$$

The filling factor P is from Kirschning and Jansen. This was found more accurate than the simpler one in Hammerstad and Jensen according to measurements reported by Deibel and Bayer.

$$P_1 = 0.27488 + U_2(0.6315 + 0.5253(0.01577B + 0)^{-20}) - 0.065683e^{-8.796U_2}$$

$$P_2 = 0.33622(1 - e^{-0.78442U_2})$$

$$P_3 = 0.0363e^{-0.66U_2} (1 - e^{-\frac{12}{10.7}U_2^{1.4}})$$

$$P_4 = 2.75(1 - e^{-\frac{U_2}{15036}}) + 1$$

$$P = P_1 P_2 [FB(0.1813 + P_3 P_4)]^{0.7963}$$

Apply the filling factor to the Getsinger dispersion model for the effective permittivity and characteristic impedance at frequency F

$$\epsilon_{effF} = \epsilon_r \cdot \frac{\epsilon_r - \epsilon_{eff0}}{1 + P}$$

$$Z_{c,F} = Z_0 \left(\frac{\epsilon_{eff0}}{\epsilon_{effF}} \right)^{0.5} \frac{\epsilon_{effF} - 1}{\epsilon_{eff0} - 1}$$

GLOSSARY

- CMP.** Chemical mechanical planarization, a method to polish the surface of a substrate.
- De-embedding.** An algorithm used to remove the electrical effects of the test equipment
- DUT.-** Device under test
- Error boxes.** Referring to the X and Y matrices used to de-embed a device measurement
- Forward Power.** The amount of power that the generator is producing and is trying to send into the load
- IC.** Integrated circuit
- Microstrip transmission line.** A small metal line used to transmit high frequency electromagnetic waves.
- LBW.** Laser beam writer, a machine used for lithography
- Load power.** The amount of power that is actually delivered to the load
- Lossy.** Electrical energy dissipation due to dielectric relaxation damping and conductance
- RC time delay.** The time it takes a circuit to change from a low voltage state to a high voltage state or visa versa. The time delay is proportional to the resistance and capacitance of the circuit.
- Reflected power.** The amount of power that is “bounced back” from the load. Reflected power results when the load impedance is not matched to the generator's requirements.
- RIE.** Reactive ion etching, a low pressure method for etching a material using a plasma containing chemical reactive species.
- S-parameter.** The Ratio of the forward and reflected waves in a transmission line
- T-parameter.** Transmission parameter, the T-parameter is related to the s-parameter by Equation 3

TRL calibration. A method of calibrating a vector network analyzer and microwave probe station using a thru line, reflect, and line of known characteristics.

VNA vector network analyzer, a device used to measure the s-parameters of an electrical network

BIBLIOGRAPHY

1. R. B. Marks and D. F. Williams, "A General Waveguide Circuit Theory," *J. Res. Natl. Inst. Stand. Technol.*, vol. 97, pp. 533-562, Sept.-Oct. 1992.
2. D. F. Williams, R. B. Marks, and A. Davidson, "Comparison of On-Wafer Calibrations," *pub. of Natl. Inst. Stand. Technol.*, pp. 1-13.
3. G. G. Engen and C. A. Hoer, "Thru-Reflect-Line," *IEEE Trans. Microwave Theory Tech.*, vol. MTT-27, pp. 987-993, 1979.
4. M. Mrozowski and J. Mazur, "Matrix Theory Approach to Complex Waves," *IEEE Trans. Microwave Theory Tech.*, vol. 40, pp. 781-785, 1992.
5. R. B. Marks, and D. F. Williams, "Characteristic Impedance Determination Using Propagation Constant Measurement," *IEEE Microwave and Guided Wave Letters*, vol. 1, no. 6, pp. 141-143, June 1991.
6. J. S. Kasten, M. B. Sterr, and R. Pomerleau, "Enhanced Through-Reflect-Line Characterization of Two-Port Measuring Systems Using Free-Space Capacitance Calculation," *IEEE Trans. Microwave Theory Tech.*, vol. 38, no. 2, pp. 215-217, February 1990.
7. M. D. Janezic, D. F. Williams, V. Blaschke, A. Karamcheti, and C. S. Chang, "Permittivity Characterization of Low-k Thin Films From Transmission-Line Measurements," *IEEE Trans. Microwave Theory Tech.*, vol. 51, no. 1, pp. 132-136, January 2003.
8. D. F. Williams, U. Arz, and H. Grabinski, "Accurate Characteristic Impedance Measurement on Silicon," *pub. of Natl. Inst. Stand. Technol.*, pp. 1-4.
9. Garrett, C.H. "Fabrication and Magnetic Properties of Patterned Thin Films" M.S. Thesis, Southwest Texas State University
10. P. H. Yih, V. Saxena, and A. J. Steckl, "A Review of SiC Reactive ion Etching in Fluorinated Plasmas," *Phys. Stat. Sol.*, vol. 202, pp. 605-642, 1997.
11. D. L. Flamm and G. K. Herb, *Plasma Etching: An Introduction*, Eds. D. M. Manos and D. L. Flamm, Chapt. 1, Academic Press, New York, 1989.
12. J. W. Coburn and E. Kay, *IBM J. Res. Develop.*, vol. 23, pp. 33, 1979.
13. T. M. Mayer and R. A. Barker, *J. Vacuum Sci. Technol.*, vol. 21, pp. 757, 1982.
14. W. S. Pan and A. J. Steckl, *J. Electrochem. Soc.*, vol. 137, pp. 212, 1990.
15. J. A. Powell, L. G. Matus, and M. A. Kuczmarski, *J. Electrochem. Soc.*, vol. 134, pp. 46, 1987.
16. R. Legtenberg, H. Jansen, M. de Boer, and M. Elwenspoek, *J. Electrochem. Soc.*, vol. 142, pp. 2020, 1995.
17. T. Syan, B. J. Baliga, and R. W. Hamaker, *J. Electrochem. Soc.*, vol. 138, pp. 3076, 1991.
18. J. W. Palmour, R. F. Davis, T. W. Wallett, and K. B. Bhasin, *J. Vacuum Sci. Technol.*, vol. A4, pp. 590, 1986.
19. R. B. Marks, "A multi-line method of network analyzer calibration," *IEEE Trans. Microwave Theory and Tech.*, Vol. 39, pp. 1205-1215, 1991.
20. K. R. Williams, "Etch Rates for Micromachining and IC Processing," *U.C Berkeley Microfabrication laboratory*, vol. 44, July 1996.

21. D. F. Williams and R. B. Marks, "Transmission Line Capacitance Measurement," *IEEE Microwave and Guided Wave Letters*, vol. 1, no. 9, pp. 243-245, September 1991.

VITA

Kevin Patrick Radican was born in Manchester, Connecticut, on March 17, 1976, the son of David and Esther Radican. Kevin relocated to Dallas, Texas, in 1988, and graduated from Edward S. Marcus High School in 1994. He moved to and Austin, Texas, in 1995, and completed a Bachelor of Science degree from Southwest Texas State University in 2000. He then entered the graduate program at Southwest Texas State University.

Permanent Address: 1606 Harvey St.
 Austin TX, 78702

This thesis was typed by Kevin Patrick Radican.

1918

Continued on next page